Efficient Preparation of Large-size Graphene Oxide Sheet and its Mosaic-like Monolayer

Jung-woo Kim

Energy Conversion and Storage Major
Interdisciplinary School of Green Energy
Graduate School of UNIST

2013

Efficient Preparation of Large-size Graphene Oxide Sheet and its Mosaic-like Monolayer

Jung-woo Kim

Energy Conversion and Storage Major
Interdisciplinary School of Green Energy
Graduate School of UNIST

Efficient Preparation of Large-size Graphene Oxide Sheet and its Mosaic-like Monolayer

A thesis
submitted to the Interdisciplinary School of Green Energy
and the Graduate School of UNIST
in partial fulfillment of the
requirements for the degree of
Master of Science

Jung-woo Kim

02. 20 . 2013 [Month/Day/year of submission]
Approved by

_____

Major Advisor
Hyoen Suk Shin

Efficient Preparation of Large-size Graphene Oxide Sheet and its Mosaic-like Monolayer

Jung-woo Kim

This certifies that the thesis of Jung-woo Kim is approved.

02. 20. 2013 [Month/Day/year of submission]

signature

_____

Thesis supervisor: Hyoen Suk Shin

signature

_____

Jong-Beom Baek

signature

_____

Yongseok Jun

ABSTRACT

The thesis focuses on the high-yield preparation of graphene oxide (GO) by the intercalation of tetrabutylammonium hydroxide (TBAOH) into graphite oxide and its mosaic-like monolayer. GO has a layered structure with many oxygen-containing groups. Thus, GO has been a graphene-like material but also used as based material for a variety of chemical modification. The large size GO sheets could be separated from graphite oxide by centrifugation, but the yield was very low. By intercalation of TBA into graphite oxide, large size GO sheets could be obtained in high yield. Furthermore, TBA-treated GO formed mosaic-like monolayer by a simple spin-coating on substrate. The XRD pattern of TBA-intercalated graphite oxide was identical to pattern for the GO in water as a form of single sheets, indicating that graphite oxide could be efficiently exfoliated by intercalation of TBA. The single sheet yield of TBA-treated graphite oxide approximately 48%, while that of graphite oxide without TBA intercalant was only 18%, the layer thickness of TGO and GO were 1.29 and 0.93nm, respectively, which indicates TBA residues on GO sheets, the existence of TBA was identified by using EA and XPS. It confirms the existence of TBA on GO sheet. The existence of TBA on GO sheets was also identified from element analysis and XPS. Interestingly, the morphology of spin-coated TGO film on hydrophilic substrates such as SiO_2 wafer and quartz formed a mosaic-like monolayer. This mosaic-like TGO monolayer also formed on hydrophobic substrates such as CVD grown graphene and Cu foil It assembled out the adsorption of TBA on GO creates low electrostatic repulsion between neighboring sheets, which helps the formation of mosaic-like monolayer by preventing overlapping of sheets. The external reflection FTIR spectroscopy study showed that the mosaic-like TGO monolayer fabricated by the simple spin-coating have same molecular orientation of functional groups as Langmuir-Blodgett film which is a typical method to make a monolayer with specific orientation of functional groups.

Contants

List of Tables

List of Figures

Figure 6. Schematic of the Langmuir–Blodgett deposition process. (a) The amphiphile is dissolved in an organic solvent and subsequently spread at the air–water interface. The solvent evaporates and a monolayer of the amphiphile at the air–water interface remains. (b) The monolayer at the air–water interface can be further manipulated by means of a movable barrier allowing control of the area per molecule. (c) The Langmuir monolayer can be transferred by an up-stroke on to a hydrophilic surface. (d) Langmuir-Blodgett trough. (e) Schematic Π-$\hat{A}$ isotherms showing tow common types of behavior, and the four main phases: S, Lc, Le, and G. Areas are roughly those for single chain amphiphiles.

Figure 7. (a) Model for C_8K according to Rudorff and Schulze (1954) showing the stacking of graphite layers (networks of small solid balls) and of potassium layers (networks of large hollow balls). The graphite and intercalate layers are arranged in an AαAβAγAδ stacking sequence, where A refers to the graphite layers and the Greek letters to the intercalate layers. (b) Schematic diagram illustrating the staging phenomenon in graphite-potassium compounds for stages $1 \leq n \leq 4$. The potassium layers are indicated by dashed lines and the graphite layers by solid lines connecting open circles, and indicating schematically a projection of the carbon atom positions

Figure 8. XRD patterns of graphite oxide. (a) Wet state of TBA intercalated graphite oxide; (b) Graphite oxide and TBA intercalated graphite a dried at 25℃ for 2day

Figure 9. Characterization of graphene from TBA intercalated graphite oxide (TGO) and graphite oxide (GO). (a) Histogram of TGO sheet size. (Average size is 21.24± 9.11 μm.), (b) Histogram of TGO sheet size. (Average size is 18.4 ± 8.35 μm.), (c, e) Tapping mode atomic force microscopy images of GO and TGO, (d, f) The height profiles of GO and TGO. The corresponding thickness of GO and TGO sheets are 0.990 nm and 1.291 nm

Figure 10. XPS of GO (a, b) and TGO (c, d), photograph of GO and TGO solution

Figure 11. UV-vis of GO and TGO solution

Figure 12. SEM of GO spin-coated film (a), TGO spin-coated film (b), TGO spin-coated film after water rinsing (e) and TGO spin-coated film with different concentration (d-f)

Figure 13. SEM of mosaic-like TGO film on Si wafer (a), CVD-grown graphene (b), Cu foil (c) and Au/Si wafer (d)

Figure 14. Sheet resistance and transmittance of TGO film after annealing in H_2 and Ar atmosphere at 1050 ℃. The top image shows a photograph for 1-5 coating of TGO deposited on a quartz substrate after annealing

Figure 15. Surface pressure-Area isotherm of GO (a) and TGO (b), SEM image of GO layers and TGO layers collected on a silicon dioxide substrate at different stage of isothermal compression. (insert)

Figure 16. Histogram for sheet size distributions of GO film and TGO film fabricated by spin-coating and Langmuir-Blodgett

Figure 17. FT-IR reflection spectra of GO film (a) and TGO film (b)

1. Introduction

1.1. Carbon allotropes

The Sixth in the periodic table of elements is, at the same time, among the most important ones. With about 180ppm, Carbon is only 17th on the list of terrestrial elements frequency, situated even after barium (Ba) or sulfur (S) – for comparison, the second-most frequent element, silicon (Si), is about 1300 times as abundant as carbon. Still the latter is essential for the assembly of all organic matter. It is predestined for this central role especially due to its mid position in the periodic system and its associated ability to form stable substance with more electropositive and more electronegative reaction partners. Yet in the present context the organic chemistry resulting from these various bonding possibilities will only be mentioned if it is employed to modify carbon materials or, to put it in other words, the element itself as a material will be in the focus. Formerly, only graphite and diamond had been known as the allotropes of carbon. But since 1985, when fullerene was discovered,1 the existence of new carbon allotropes which have nanoscale size has been demonstrated. Fullerene, carbon nanotube,[2] graphene,[3] which are 0D, 1D, 2D nanostructure respectively, were discovered sequentially, and they have unique electric properties distinguished with the existing carbon allotropes due to quantum confinement effect. Because of these unique properties, they have been greatly studied for last two decades.

The idea of cage-like carbon structure is by far not as new as one might believe. First theoretical considerations date back to the year 1966. Scientist D.E.H. Jones, who chose himself the pseudonym Daedalus, published theoretical treatises on fullerene-shaped objects. However, no attention of any kind was bestowed upon his speculations about hollow structure entirely made from carbon atoms. A first theoretically substantiate paper on C_{60} was published by E. Osawa in 1970. He let himself be inspired by his son's soccer ball while reflecting on super-aromatic π-systems and postulated an analogous structure with icosahedra symmetry for the C_{60}-molecule, predicting its stability from Hückel calculations. He saw that corannulene, synthesized shortly before by Barth and Lawton, had to be a partial structure of that cage (Figure 1). His publications as well were granted due attention only after the experimental discovery of fullerenes. Even though they are not theoretical treatise themselves, the buildings of the American architect Richard Buckminster Fuller (1895-1983) were some structural inspiration nevertheless. His geodetic domes, self-supporting cupolas consisting of various polygons, show similar structural feature like the carbon cages, and it was to his honor that the latter were named "fullerenes" or be a partial structure of that cage (Figure 1). His publications as well were granted due attention only after the experimental discovery of fullerenes. Even though they are not theoretical treatise themselves, the buildings of the American architect Richard Buckminster Fuller (1895-1983) were some structural inspiration nevertheless. His geodetic domes, self-supporting cupolas consisting of various polygons, show similar structural feature like the carbon cages, and it

was to his honor that the latter were named “fullerenes” or “Buckminsterfullerenes”. Still it had already been in the early twenties that the first geodetic dome was realized by the German architect W. Bauersfeld, but he failed to label his structure with a catching name, and so today such edifices are inevitably connected to the name of Fuller. It was mainly in the sixties and seventies when a number of buildings were erected taking up Fuller’s concept. One of the most impressive examples is the USA pavilion at the 1967 World Expo. Microorganisms of the class of diatoms represent another example of a structural relation. These algae grow in structures that correspond to 100,000-fold enlarged fullerene cages (Figure 1(c)) with the polygons on their surface exhibiting the same distribution as observed for fullerene. In 1985, the world of the element carbon was deemed an exhaustively explored and mature field of research. For the most important allotropes, the essential properties were known as well as the interconnections between them, and apart from Organic Chemistry, the elemental chemistry of carbon was thoroughly examined, too. Then came the day when a signal at 720 *m/z* in a mass spectrum of “new” carbon allotropes had begun.

A year before that, first experimental result had already suggested the existence of certain carbon cluster. In experiments on laser-evaporation of graphite, signals attributable to the cluster of 30 to 190 carbon atoms had been detected in the time-of-flight mass spectrum. Most peculiar was the fact that only even numbers of atoms had been observed. Still for the time being, the clusters’ structure had not been elucidated. H. W. Kroto, J. R. Heath, S. C. O’Brien, R. F. Curl, and R. Smalley then made the decisive breakthrough in the discovery and identification of fullerenes when attempting to simulate stellar conditions namely those in the class of Red Giants. Their experiment considered in focusing a pulsed laser beam on a target of graphite under a stream of helium and subsequently analyzing the resulting particles in a mass spectrometer. As expected, they mainly detected molecules with compositions of HC_7N and HC_9N, which are also prevalent in space, but on modifying the experimental conditions, they suddenly found the spectra dominated by a signal at *m/z* 720. Yet another peak at *m/z* 820 was observed, which relates to C_{70}. They concluded that they had found a C_{60} molecule with highly symmetric cage structure. For this breakthrough work Nobel prizes was awarded to Kroto, Smalley, and Curl. Still this first evidence did not constitute a suitable method to supply sufficient quantities for an investigation on physical and chemical properties of the new substrate. It was only in 1990 when the groups of W. Krätschmer and D. R. Huffman succeeded in isolating macroscopic amounts of the most abundant fullerene C_{60} by the arc evaporation of graphite or by resistance heating of graphite electrode, respectively. In fact, their initial intention too had been to produce in the laboratory substance that exists in interstellar dust. At suitable conditions, their IR-spectra exhibited four sharp, characteristic signals that related to those predicted for the C_{60} molecule. Later on, C_{70} and higher fullerene were also obtained. The first description of fullerene containing one or more atoms within the cage followed soon after the detection of the fundamental structure. This so-called endohedral fullerene played a crucial part in the isolation of higher fullerenes.

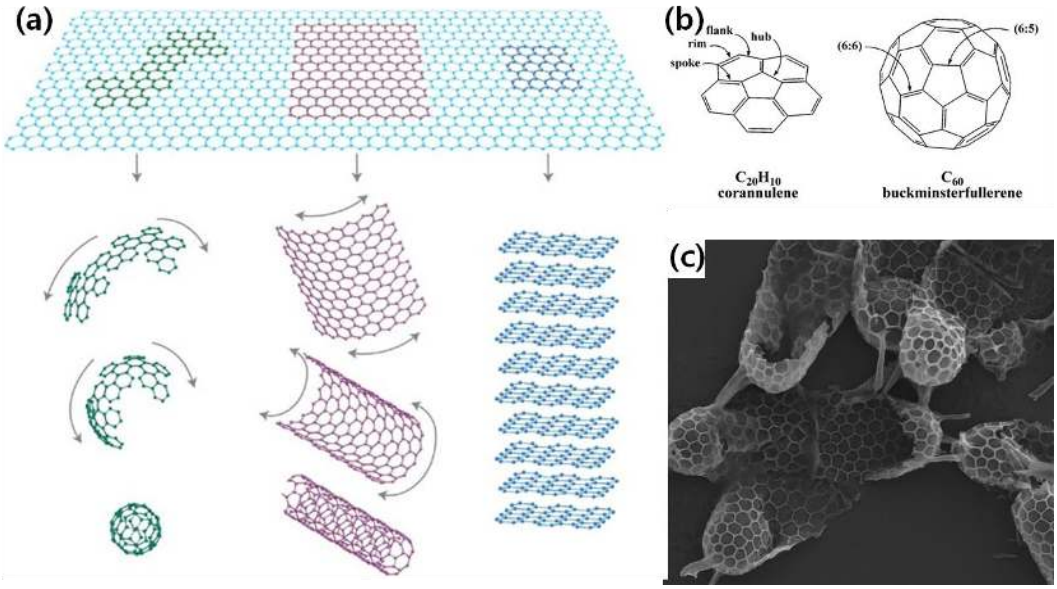

Figure 1. (a)Graphene; the mother of all graphitic forms, (b) Corannulene and C_{60} and (c) The diatom Stephanopyxis turris

Carbon fibers have been known for long. They are being used as a variety of materials for mechanical reinforcement and to make the respective composites more resistant to different external influences. Carbon-reinforced materials for sports gear, like the frames of tennis racket or mountain bike, are but a few examples. A closer look on the employed carbon fibers in the electron microscope reveals that at least some of these long, thin objects possess a tube-shaped core measuring several nanometers across. Then the outer layers of the fiber are arranged around this central cavity. In 1976, M. Endo and co-workers reported on concentric, tubular structures in the core of carbon fibers and postulated a catalytic growth mechanism. These reports, however, were paid attention again only after the group of S.Iijima had found carbon nanotubes when studying different soot types from arc-discharge experiments for fullerene production. Upon examination in the transmission electron microscope, area of equidistant lines symmetrically arranged around a central void was observed. They soon realized that these stripes were the projection of tubular objects. Consequently the observed structures had to be tubes fitted one into another (Figure 2(a), 2(b)). Later on, the same group went on to describe single-walled carbon nanotubes (SWNTs) that had been obtained after modifying the preparative conditions. Soon it became evident that these nanotubes were closely related to the fullerene that had been known since 1985. Theoretical predictions of carbon nanotubes are largely unknown in the literature. Still there are collections of publications on the structure of carbon nanofibers which basically include in their discussion on the tubular core of the fibers. However, these facts were largely ignored until after the discovery of carbon nanotubes because it seemed unlikely ever to be able to obtain the isolated core of such a fiber. The carbon nanotubes also have a lot of structural features in common with the carbon cage described in fullerene. Contrasting some fullerene species, however, they do not occur naturally in any form, neither on earth nor in space, so they are a completely artificial form of carbon indeed. In any case they exhibit bent graphene layers, but while the whole three spatial directions are affected in the fullerenes, the curvature is limited to two dimensions here. Hence, the incorporation of five membered rings – indispensable to achieve closure of the bowl in fullerenes – is unnecessary for the construction of nanotubes. It suffices to bend the graphene sheet from its plane and make it a cylinder. Compared to fullerenes of equal diameter, nanotubes consequently bear less strain their carbon atoms exhibit a smaller degree of sp^3-hybridization. However, considering the caps of closed carbon nanotubes reveals that these are partially made from fullerene fragments. For example, the (5,5)- and (9,0)-nanotubes presented there are terminated by suitably oriented fullerene hemispheres. A cylindrical tube is situated between them. Hypothetically reducing its length to zero leads to contact of the caps and establishes an intact molecules of C_{60}. The naming of specific carbon nanotubes is based on using a pair of numbers that indicate the coiling direction and the perimeter of the tube. This pair of descriptors (n,m) results from geometrical considerations. It is considered as an extreme of closed nanotubes without cylindrical

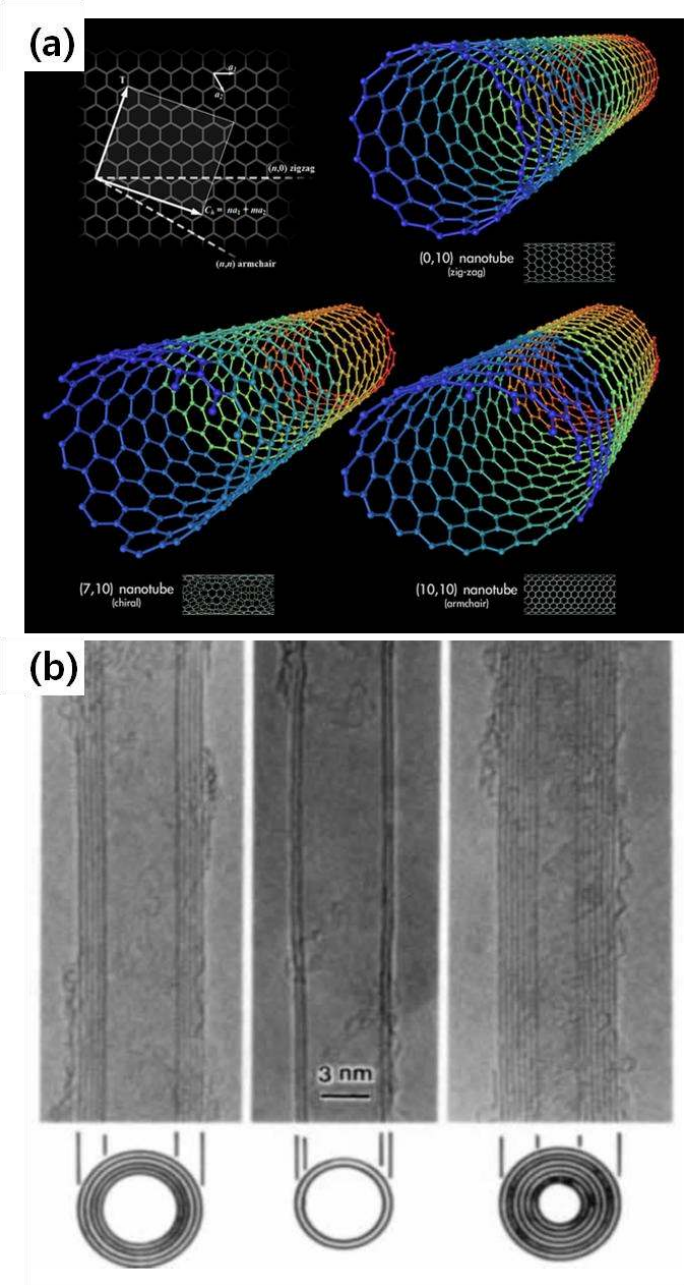

Figure 2. (a) Different types of carbon nanotubes result from formal rolling up of a graphene layer and (b) HRTEM image of Mutiwalled carbon nanotubes

centerpiece. The question arose before whether carbon nanotubes are an elemental modification in their own right. Modifications of a given material or element are, by definition, substances identical in chemical composition (pure carbon in this case), but different in crystal structure. This phenomenon is also called allotropy. The different lattices result in distinct properties and varied stabilities regarding temperature and pressure. At given values of these parameters there is usually but one modification that is thermodynamically stable. Suitable treatment may convert it into other allotropes. Graphite is the most stable form of carbon at standard conditions. However, this does not mean that any other modification of carbon spontaneously transforms into graphite at room temperature and normal pressure. The activation barrier for these conversions is high enough to let metastable materials exist under normal conditions. Diamond is the most prominent example of this effect. Now, does nanometer represent a modification of their own or not? There are two fundamentally opposite opinions on the matter, both of which shall be considered here. Nanotubes exhibit the same elemental composition as any other material from pure carbon and, at the same time, feature distinct electronic and mechanical properties. In this respect they might surely be considered as an autonomous modification of carbon. The question of different crystal structures, however, cannot unambiguously be answered. The bonding in a carbon nanotube is based on the same pattern as in graphite; in particular the structure of a graphene layer is obviously related to that of the carbon framework in a nanotube. Altogether they might simply be regarded as bent graphene sheet, and in multi-walled nanotubes the neighboring sheets are even connected via π-π interactions, so basic structural features of graphite are present in carbon nanotubes as well. From this point of view, one might argue that nanotubes are a heavily distorted variant of graphite (or that graphite represents an extreme of nanotubes with infinitesimally low curvature). Each nanotube may further be described as a result of rolling up a graphene layer under a certain angle and structure, one might just as well argue that there is an infinite number of nanotube modifications (provided that their length and diameter could also be infinite). The same ambiguity must be started for the fullerenes that exist in different sizes, too. Using a strict interpretation of the definition regarding distinct crystal structures, solids of C_{60}, C_{70} and any other fullerene would each would be a modification of their own. It is virtually impossible to name carbon nanotubes correctly according to IUPAC nomenclature for two reasons. Firstly, the number of carbon atoms constituting the nanotube is enormous – it might be tens or hundreds of thousands. Secondly it would be extremely difficult to apply the classical nomenclature of organic compounds. A whole new system has consequently been established to classify carbon nanotubes. It is perfectly apt to distinguish different structures, and it even permits to infer certain properties of the species at hand from the components of its name. There are three classes of carbon nanotubes differing in the way the basic graphene sheet is rolled up (Figure 4):

- Zig-zag carbon nanotubes

  The graphene layer is rolled up in a way to make the ideal ends of open tube be a zig-zagged

edge. It means that the rolling up is done in parallel to the unit vector of the graphene lattice.

- Arm-chair carbon nanotubes

  In comparison to the zig-zag tubes, the graphene sheet is turned by 30^o before rolling up. The perfect terminus is an edge consisting of the sides of the last row of six-membered rings.

- Chiral carbon nanotubes

  If the angle of turning the graphene layer before rolling up is between 0^o and 30^o, chiral nanotubes are obtained. They are characterized by a line parallel with the unity vector that spirals up around the tube. Consequently two enantiomeric forms exist for these species.

1.2. What is graphene?

Graphene, one-atomic-thick sheet of sp^2 hybridized and 2-dimensional honeycomb carbon lattice crystal and mother of other carbon allotropes such as CNT, C_{60} and graphite, is first isolated from bulk graphite by Andre Geim in 2004 (Figure 3(a)).[3] But the term 'graphene' was first used in 1987 to describe single sheet of graphite as one of the constituents of graphite intercalation compounds (GICs).[4] It was also used in early descriptions of carbon nanotubes and epitaxial graphite.5 The single-layer of graphite was previously grown epitaxial on top of various materials. This 'epitaxial graphene' consists of a single-atom-thick hexagonal lattice of sp^2-bonded carbon atoms, but the hybridization between *d* orbital of substrate and π orbital of graphene alters the electronic structure of epitaxial graphene. Nevertheless, graphene, a 2D honeycomb lattice had been presumed not to exist in the 'free state' due to thermodynamic instability, being as an 'academic' material. But the free-standing graphene was unexpectedly using Scotch tape by Geim and the follow-up experiments confirmed that its charge carriers were indeed massless Dirac fermions.[6, 7] These discoveries led to the explosion of interest in graphene. In 2010, "For groundbreaking experiments regarding the two-dimensional material graphene," Andre Geim together with Konstantin Novoselov were awarded the Nobel Prize in Physics. There are two important features in the structure and electronic propertied of graphite: a two-dimensional layered structure and an amphoteric feature (Kelly, 1981). The basic unit of graphite, called graphene is an extreme state of condensed aromatic hydrocarbons with an infinite in-plane dimension, in which an infinite number of benzene hexagon ring are condensed to form a rigid planar sheet, as shown in Figure 3(b).

1.2.1. Electronic Properties of graphene

Graphene differs from most conventional three-dimensional materials. Intrinsic graphene is a semi-metal or zero-gap semiconductor. Understanding the electronic structure of graphene is the starting point for finding the band structure of graphite. It was realized as early as 1947 by P. R. Wallace8 that the *E-k* relation is linear for low energies near the six corners of the two-dimensional hexagonal Brillouin zone, leading to zero effective mass for electrons and holes (Figure 3(c)-(g)). Due to this

linear (or “conical") dispersion relation at low energies, electrons and holes near these six points, two of which are in equivalent, behave like relativistic particles described by the Dirac equation for spin 1/2 particles.[9, 10] Hence, the electrons and holes are called Dirac fermions,10 and the six corners of the Brillouin zone are called the Dirac points. Figure 3(d) shows the peculiar single-particle band structure of this 2D material. The linear dispersion at low energies makes the electrons and holes in graphene mimic relativistic particles that are described by the Dirac relativistic equation for particles with spin 1/2, and they are usually referred to as Dirac Fermions. Their dispersion, $E_{2D} = \hbar v_F = (k_x^2 + k_y^2)^{1/2}$, is analogous to that of photons, $E_k = \hbar ck$, but with the velocity of light c replaced by $v_F \approx 10^6$ m s^{-1}, the Fermi velocity. Thus, electrons and holes in graphene have zero effective mass and a velocity that is about 300 times slower than that of light. This linear dispersion relationship also means that quasi-particles in graphene display properties quite different to those observed in conventional three-dimensional materials, which have parabolic dispersion relationships. For example, graphene displays an anomalous quantum Hall effect and half-integer quantization of the Hall conductivity.[7, 11] The quantum Hall effect in graphene can be observed even at room temperature.[12] The discovery of isolated single-layer graphene was biggest accidental discovery in condensed-material science in 2004.[3] It allows observing the pronounced Shubnikov-de Hass oscillation in both longitudinal resistivities (ρ_{xy}). A year after first discovery, Geim[11] and Philip Kim[7] independently reported the half integer QHE occurred in single –layer graphene. Graphene was the first ideal realization of such a two-dimensional system. However, its behavior is expected to differ markedly from the well-studied case of quantum wells in conventional semiconductor interfaces such as GaAs-GaAlAs heterojunction.[13] This difference arises from unique electronic properties of graphene, which exhibits electron-hole degeneracy and vanishing carrier mass near the point of charge neutrality which is called Dirac point. Indeed, an existence of a non-zero Berry’s phase (a geometric quantum phase) electron wave function-a consequence of the exceptional topology of the graphene band structure. In order to explain the electron transport behavior in single-layer graphene, Dirac’s equation is essential. The charge carriers in graphene mimic relativistic particles with zero rest mass and have an effective ‘speed of kight’. Although there is nothing particularly relativistic about electrons moving around carbon atoms, their interaction with the periodic potential of graphene’s honeycomb lattice gives rise to new quasiparticles that at low energies E are accurately described by the (2+1)-dimensional Dirac equation with an effective speed of light $\nu_F \approx 10^6\ m^{-1}\ s^{-1}$. These quasiparticles, called massless dirac fermions, can be seen as electron that have lost their rest mass m_0 or as neutrions that acquired the electron charge e.

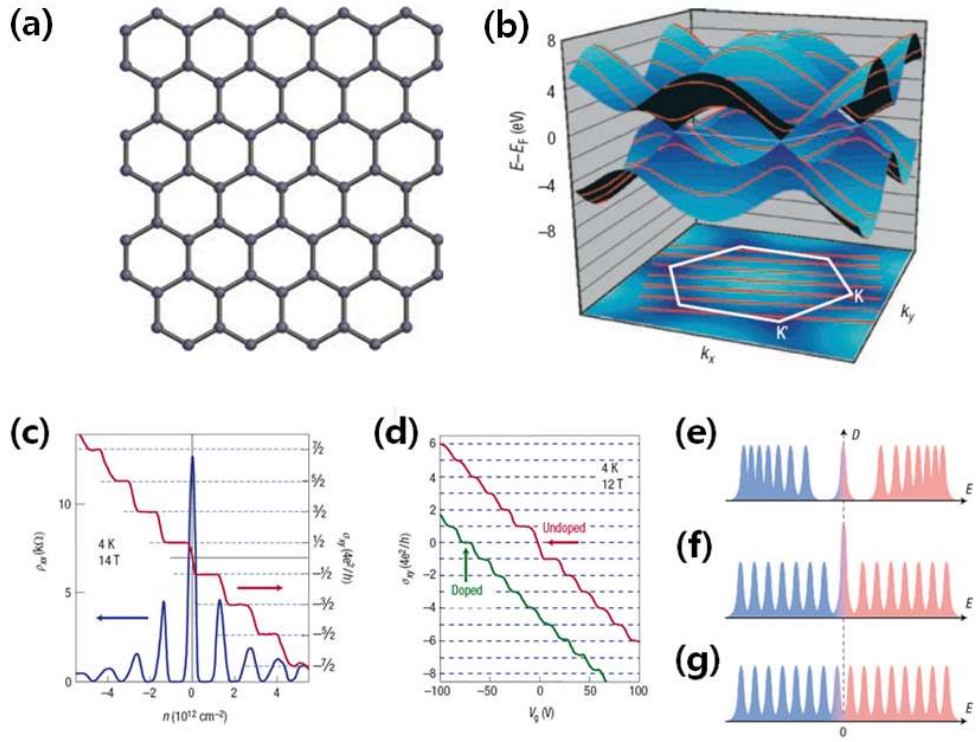

Figure 3. (a) Structure of graphene, (b) The band structure (top) and Brillouin zone (bottom) of graphene. The valence band (which is of π-character) and the conduction band (π*-character) touch at six points that lie at the Fermi energy, but only two of these points — the K and K' points — are inequivalent. At these Dirac points, the density-of-states is zero, so graphene can be considered as a zero-gap semiconductor. At low energies, the dispersion is linear, determined by the conical sections involving the K and K' points. The quantization of the circumferential momentum, k, leads to the formation of a set of discrete energy sub-bands for each nanotube (red parallel lines). The relation of these lines to the band structure of graphene determines the electronic structure of the nanotube. If the lines pass through the K or K' points, the nanotube is a metal: if they do not, the nanotube is a semiconductor. (c) The hallmark of massless Dirac fermions is QHE plateaux in σ_{xy} at half integers of $4e^2/h$. (d) Anomalous QHE for massive Dirac fermions in bilayer graphene is more subtle (red curve56): σ_{xy} exhibits the standard QHE sequence with plateaux at all integer N of $4e^2/h$ except for N = 0. The missing plateau is indicated by the red arrow. The zero-N plateau can be recovered after chemical doping, which shifts the neutrality point to high Vg so that an asymmetry gap (≈0.1eV in this case) is opened by the electric field effect (green curve). (e)–(g) Different types of Landau quantization in graphene. The sequence of Landau levels for massless Dirac fermions in single-layer graphene (e) and for massive Dirac fermions in bilayer graphene (f). The standard LL is expected to recover if an electronic gap is opened in the bilayer (g)[14]

1.2.2. Mechanical Properties of graphene

As of 2009, graphene appears to be one of the strongest materials ever tested. Measurements have shown that graphene has a breaking strength 200 times greater than steel, with a tensile strength of 130 GPa (19,000,000 psi).[15] Using an atomic force microscope (AFM), the spring constant of suspended graphene sheets has been measured. Graphene sheets, held together by van der Waals forces, were suspended over SiO_2 cavities where an AFM tip was probed to test its mechanical properties. Its spring constant was in the range 1–5 N/m and the Young's modulus was 0.5 TPa, which differs from that of the bulk graphite. These high values make graphene very strong and rigid. These intrinsic properties could lead to using graphene for nanoelectromechanical system (NEMS) applications such as pressure sensors and resonators.[16]

1.2.3. Optical Properties of graphene

Graphene's unique electronic properties produce an unexpectedly high opacity for an atomic monolayer, with a startlingly simple value: it absorbs $\pi\alpha \approx 2.3\%$ of white light, where α is the fine-structure constant.[17] (Figure 4) This is "a consequence of the unusual low-energy electronic structure of monolayer graphene that features electron and hole conical bands meeting each other at the Dirac point is qualitatively different from more common quadratic massive bands".[18] Based on the Slonczewski-Weiss-McClure (SWMcC) band model of graphite, the interatomic distance, hopping value and frequency cancel when the optical conductance is calculated using the Fresnel equations in the thin-film limit. This has been confirmed experimentally, but the measurement is not precise enough to improve on other techniques for determining the fine-structure constant. Recently it has been demonstrated that the band gap of graphene can be tuned from 0 to 0.25 eV (about 5 micrometer wavelength) by applying voltage to a dual-gate bilayer graphene field-effect transistor (FET) at room temperature.[19] The optical response of graphene nanoribbons has also been shown to be tunable into the terahertz regime by an applied magnetic field.[20] It has been shown that graphene/graphene oxide system exhibits electrochromic behavior, allowing tuning of both linear and ultrafast optical properties.

1.2.4. Thermal Properties of graphene

The near-room temperature thermal conductivity of graphene was recently measured to be between $(4.84\pm0.44) \times 10^3$ to $(5.30\pm0.48) \times 10^3$ $Wm^{-1}K^{-1}$. These measurements, made by a non-contact optical technique, are in excess of those measured for carbon nanotubes or diamond. It can be shown by using the Wiedemann-Franz law, that the thermal conduction is phonon-dominated.[21] However, for a gated graphene strip, an applied gate bias causing a Fermi energy shift much larger than k_BT can cause the electronic contribution to increase and dominate over the phonon contribution at low temperatures. The ballistic thermal conductance of graphene is isotropic.[22]

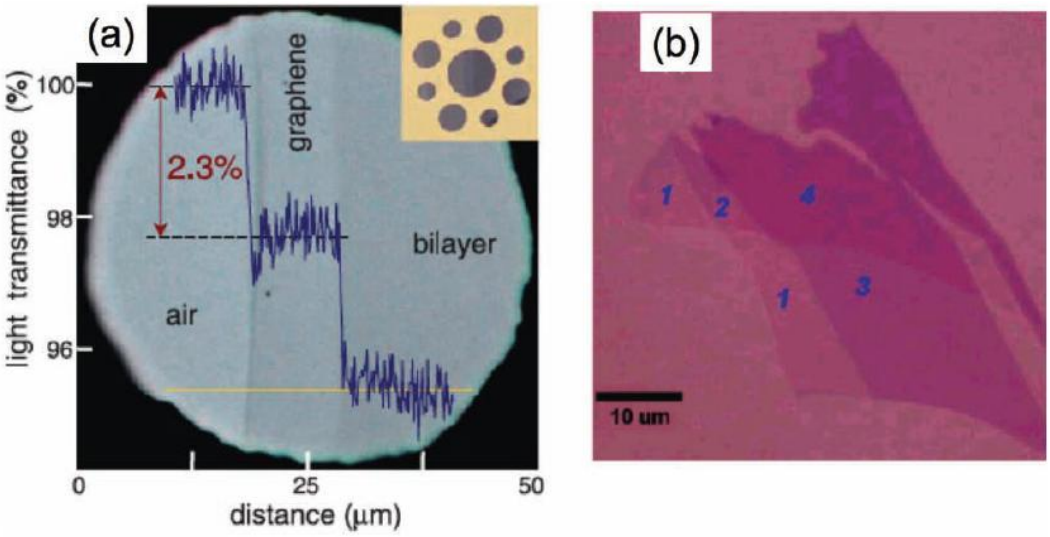

Figure 4. Optical properties of graphene. (a) Photograph of a 50 μm aperture partially covered by graphene and its bilayer. The line scan profile shows the intensity of transmitted white light along the yellow line. Inset shows the sample design: a 20 μm thick metal support structure has apertures 20, 30, and 50 μm in diameter with graphene flakes deposited over them; (b) Optical image of graphene fl akes with one, two, three, and four layers on a 285 nm thick SiO_2 on Si substrate

1.3. Graphene synthesis methods

1.3.1. Mechanical exfoliated graphene from graphite

The exfoliated graphene was first achieved by mechanical exfoliation.[3, 23] As is the case of most scientific discoveries, graphene was discovered by accident and surprisingly atomic scale thin layer graphene samples were observed by optical microscope.[3] The key for the success probably was the use of high throughput visual recognition of graphene on a proper chosen substrate, which provides a small but distinguished optical contrast. The graphene sheet made by mechanical exfoliation shows the highest crystalline and the lowest degree of defects among the graphene samples made until now and therefore it is appropriate for studies about the physical and chemical properties of graphene. However, trained eyes are required for identification of single-layer graphene.

1.3.2. Chemically converted graphene

The different method is using oxidized graphite. Exfoliated graphite oxide is called graphene oxide.[24-26] Graphene oxide is well dispersed into aqueous solution. Compared to the dispersion method in organic solvent, the yield of single-layer is quite better in case of aqueous solution. However, graphene oxide should be reduced to recover into graphene, and this process induces the aggregation of chemically reduced graphene oxide. This problem was resolved by addition of NH_3 to control of pH. This treatment remains the positive charges on reduced graphene, which prohibit the aggregation of reduced graphene oxide.[25]

1.3.3. Epitaxial growth of graphene

Another growth method is to heat silicon carbide (SiC) to high temperatures to reduce it to graphene.[27, 28] Ultrathin epitaxial graphite was grown on single-crystal SiC by vacuum graphitization. This process produces a sample size depending on the size of the SiC substrate. The face of the SiC used for graphene creation, the silicon-terminated or carbon-terminated, highly influences the thickness, mobility and carrier density of the graphene. By this method, most important properties of free-standing graphene have been visualized. It was also shown that even without being transferred graphene on SiC exhibits the properties of massless Dirac fermions such as the anomalous QHE.[28] Epitaxial graphene on SiC can be patterned using standard nanolithography techniques. In 2008, researchers at MIT Lincoln Lab have produced hundreds of transistors on single chip.[29] Hughes Research Laboratories produced monolayer graphene on SiC.[30] However, this method is economically expensive for the realization integrated circuit or large-scale transparent electrode.

1.3.4. Chemical vapor deposition

In 2008, Jing Kong in MIT[31] and Byung Hee Hong in SKKU[32] independently demonstrated the vapor method of thin film layer graphene using nickel substrate. These graphene sheets have been successfully transferred to various substrates, to indicate viability for numerous electronic applications. An improvement of this technique has been founded in copper foil where the growth automatically stops after a single layer of graphene due to low carbon solubility, and arbitrarily large graphene films can be fabricated.[33] In 2010, 30-inch graphene films for transparent electrodes have been synthesized by the same technique.[34] Carbon atoms can dissolve in the metal pool at high temperature and then segregate out to from graphene on metal surfaces when the temperature lowers. The major difference between the two metals is their carbon solubility. With a larger solubility, nickel provides a large pool due to form multi-layers on nickel but single-layer on copper. Compared with that of nickel-carbon and copper-carbon, the phase diagram of silicon-carbon is quite different. Beside an even smaller carbon solubility in Si than that in copper.[35]

1.4. Fabrication of graphene thin film

Fundamental researches have initiated from the micromechanical cleavage of highly crystalline graphite for high-quality graphene sheets. Recent efforts are geared toward producing the graphene sheets in a controlled, scalable, and reproducible manner. For example, stable suspensions of graphene oxide can be readily obtained by ultrasonication of chemically oxidized graphite oxide, offering the potential of creating large-scale graphene thin films. A number of approaches have been made to assemble these well-dispersed oxidized or chemically reduced graphene oxide nanosheets into thin films with tailorable properties. These include vacuum filtration, [36-41] dip coating,[42, 43] spin-coating,[44-47] Langmuir–Blodgett assembly,[48, 49] and direct chemical vapor deposition.[50, 51] The layer-by-by-layer assembly has been so far used to make thin films consisting of poly (acrylic acid)-modified and poly (acryl amide)-modified graphene nanoplatelets or negative-charged graphite oxide and positive-charged polymer like poly (allylamine hydrochloride).[52, 53] These layer-by-layer assemblies can create highly controllable, conformal thin films in terms of thickness, transmittance, and sheet resistance. This method affords ultrathin film of any materials with an excellent control over the optical and electrical properties the terahertz regime by an applied magnetic field.[20] It has been shown that graphene/graphene oxide system exhibits electrochromic behavior, allowing tuning of both linear and ultrafast optical properties.

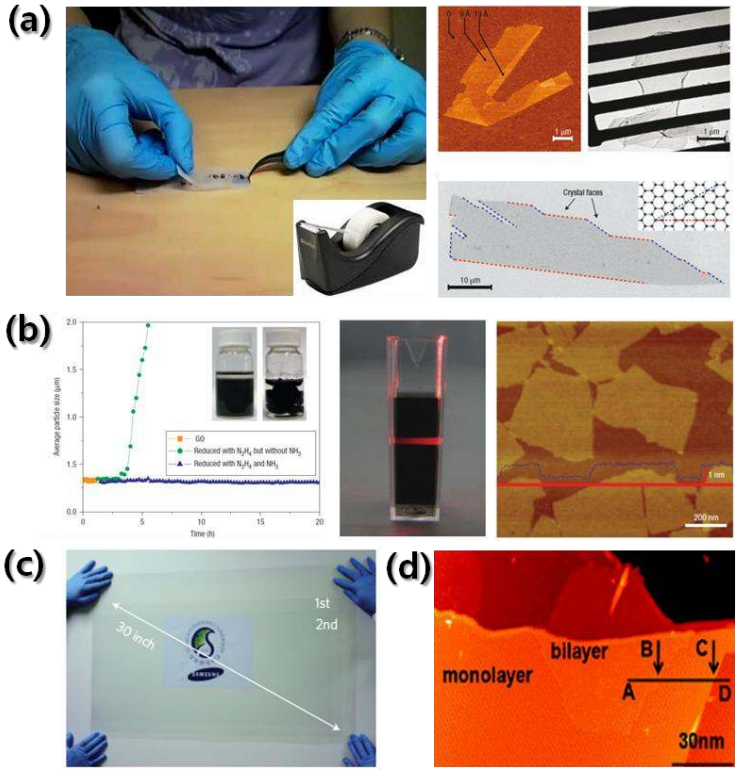

Figure5. Different types of Graphene. (a) Mechanically exfoliated graphene from graphite, (b) chemically converted graphene, (c) large area CVD-grown graphene and (d) epitaxial grown graphene on SiC

1.4.1. Langmuir-Blodgett film

The term 'Langmuir films' is molecular monolayers at the liquid-gas interface and the term 'Langmuir-Blodgett films(LB)' is monolayer and multilayer deposited from the liquid-gas interface onto a solid substrate. In order to form a Langmuir film it is necessary for a substance to be insoluble in water but for each of its molecules to have a hydrophilic region which will preferentially reside on the water surface. A long chain carboxylic acid is an ideal example of such a substance. The long hydrocarbon 'tail' is hydrophobic and the acid head group, -COOH, is, even if un-ionized, hydrophilic.[54] The first step of the LB deposition process is the formation of a well defined monolayer at the air–water interface. These so-called Langmuir monolayers are a precursor film within the LB fabrication. The preparation process is illustrated schematically in Figure 6. The amphiphile is dissolved in an organic solvent and subsequently spread at the air–water interface. The solvent evaporates and a monolayer of the amphiphile at the air–water interface is then produced. These Langmuir monolayers can be further manipulated by means of a moveable barrier which allows us to control the area per molecule.[55]

Among the many techniques employed in the characterization of Langmuir monolayers, the surface pressure and the surface potential methods have been the most widespread.

Surface pressure is defined as the decrease in the surface tension of the liquid owing to the presence of the monolayer. It is normally measured using a Wilhelmy plate/electrobalance arrangement that monitors the force required for the sensing plate to be kept stationary against changes in surface tension. The pressure-area (Π-A) isotherm, obtained by compressing the monolayer, is the most commonly used characteristic in the description of a monolayer. When the monolayer is compressed beyond the steep increase in surface pressure, collapse occurs and the molecules are forced out of the monolayer forming lenses. From the shape of such isotherms it is possible to recognize four principal monolayer phases: a gaseous (G) phase, a liquid-expanded (Le) phase, a liquid-condensed (Lc) phase, and a so-called solid (S) phase. These phase are illustrated in the schematic isotherms shown in Figure 6 (e).[56] In the gaseous state, the molecules are far enough apart on the water surface that they exert little force on one another. As the surface area of the monolayer is reduced, the hydrocarbon chains will begin to interact. The liquid state generally called the expanded monolayer phase. The hydrogen chains of the molecules in such a film are in a random, rather a regular orientation, with their polar groups in contact with the subphase. As the molecular area is progressively reduced, condensed phase may appear. There may be more than one of these and the emergence of each condensed phase can be accompanied by constant pressure regions of the isotherm, as observed in the cases of a gas condensing to a liquid and a liquid solidifying. These regions will be associated with enthalpy changes in the monolayer. In the condensed monolayer states, these molecules are closely packed and are oriented with the hydrocarbon chain pointing away from the water surface. The surface pressure continues to increase with decreasing surface area until a point

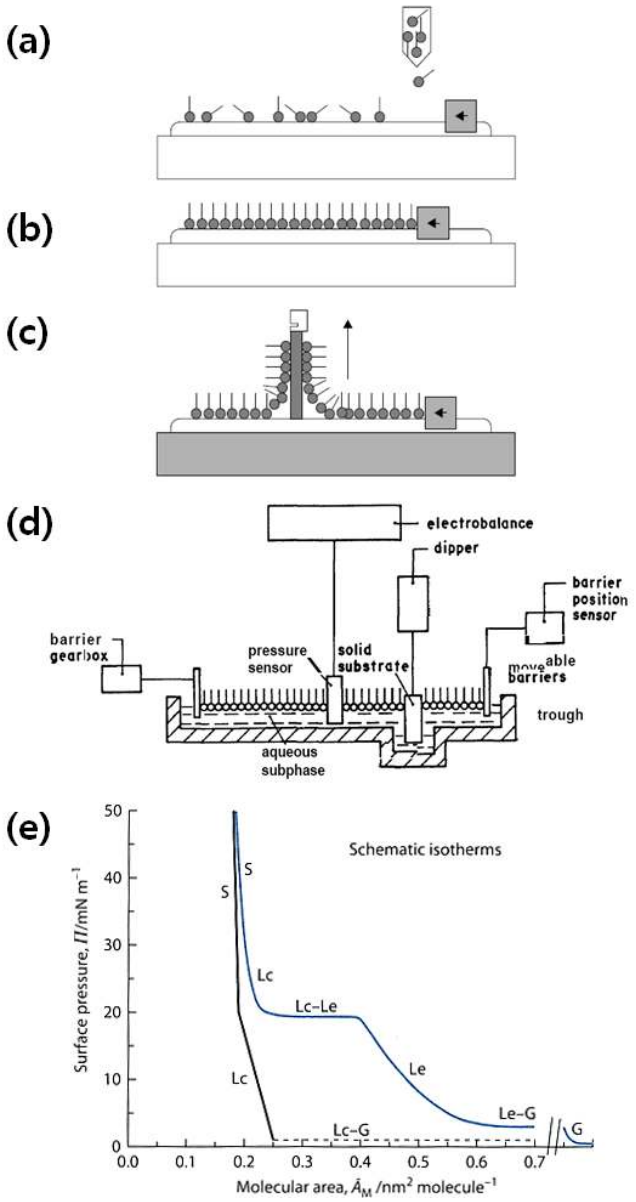

Figure 6. Schematic of the Langmuir–Blodgett deposition process. (a) The amphiphile is dissolved in an organic solvent and subsequently spread at the air–water interface. The solvent evaporates and a monolayer of the amphiphile at the air–water interface remains. (b) The monolayer at the air–water interface can be further manipulated by means of a movable barrier allowing control of the area per molecule. (c) The Langmuir monolayer can be transferred by an up-stroke on to a hydrophilic surface. (d) Langmuir-Blodgett trough. (e) Schematic Π-$\hat{A}$ isotherms showing tow common types of behavior, and the four main phases: S, Lc, Le, and G. Areas are roughly those for single chain amphiphiles. Note that the G phase occurs at much larger areas than shown. [56]

is reached where it is not possible to increase the pressure any further and the area of the film decrease if the pressure is kept constant, for the pressure falls if the film is held at constant area. This is referred it as collapse.[57]

1.5. Intercalation reaction

1.5.1. Intercalation of graphite

Graphite intercalation compounds are formed by the insertion of atomic or molecular layers of a different chemical species called the intercalant between layers in a graphite host material, as shown in Figure 7. The intercalation compounds occur in highly anisotropic layered structures where the interplanar binding forces are large in comparison with the interplanar binding forces. The most common examples of host materials for intercalation compounds are graphite and the transition metal dichalcogenides. Of the various types of intercalation compounds, the graphite compounds are of particular physical interest because of their relatively high degree of structural ordering. The most important and characteristic ordering property of graphite intercalation compounds is the staging phenomenon, which is characterized by intercalate layers that are periodically arranged in a matrix of graphite layers. Graphite intercalations compounds are thus classified by a stage index *n* denoting the number of graphite layers between adjacent intercalate layers, as is illustrated in Figure 7. This staging phenomenon is general phenomenons in graphite intercalation compounds, even in those samples with very dilute intercalate concentrations (n ~10). Intercalation provides to the host material a means for controlled variation of many physical properties over wide ranges. Because the free carrier concentration of the graphite host is very low (10^{-4} free carriers/atom at room temperature), intercalation with different chemical species and concentrations permits wide variation of the free carrier concentration and thus of the electrical, thermal and magnetic properties of the host material. Of these properties, the effect of intercalation on the electrical conductivity has probably attracted the greatest amount of attention because of the fabrication of an intercalation compound (C_XAsF_5) with a reported room temperature conductivity exceeding that of copper (Foley et al. 1977). Perhaps even more striking is the range of electrical conductivity behavior, ranging from almost insulating behavior for the c-axis conductivity in certain acceptor compounds to superconducting in-plane behavior below 1.0 K for the first stage alkali metal donor compounds C_8K where neither of the parent chemical species individually exhibit superconductivity (Hanney et al. 1965, Koike et al. 1978). The large increase in conductivity in intercalated graphite results from a charge transfer from the intercalate layer where the carriers have a low mobility to the graphite layers where the mobility is high. Since the most significant modifications to the graphite involve graphite layers adjacent to the intercalate layer, it is convenient to distinguish between the graphite bounding layers adjacent to the intercalant, and the graphite interior layers that have only graphite nearest-neighbor layers.

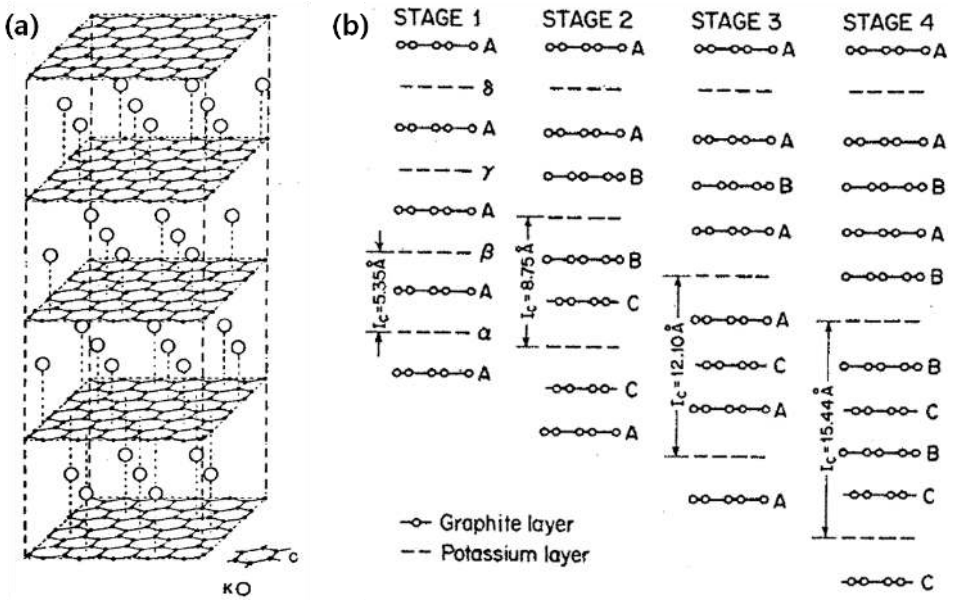

Figure 7. (a) Model for C_8K according to Rudorff and Schulze (1954) showing the stacking of graphite layers (networks of small solid balls) and of potassium layers (networks of large hollow balls). The graphite and intercalate layers are arranged in an AαAβAγAδ stacking sequence, where A refers to the graphite layers and the Greek letters to the intercalate layers. (b) Schematic diagram illustrating the staging phenomenon in graphite-potassium compounds for stages $1 \leq n \leq 4$. The potassium layers are indicated by dashed lines and the graphite layers by solid lines connecting open circles, and indicating schematically a projection of the carbon atom positions

The synthesis of a graphite intercalation compound was first reported by Schaffautl (1841). However, the first systematic studies of these compounds began in the early 1930s with the introduction of X-ray diffraction techniques for stage index determinations (Hoffman and Frenzel 1931, Schleede and Wellman 1932). Though the systematic study of their physical properties began in the late 1940s, it is only in recent years that research on graphite intercalation compounds has become a field of intense activity internationally. A large number (>>100) of reagents can be intercalated into graphite. These intercalants are commonly classified according to whether they form donor or acceptor compounds. The most common and most widely studied of the donor compounds are the alkali metal compounds with K, Rb, Cs and Li, though other donor intercalants are known, such as alkaline earth metals, lanthanides and metal alloys of these with each other or with alkali metals. Ternary donor intercalation compounds have also been prepared using alkali metals with hydrogen or polar molecules, such as ammonia and tetrahydrofuran, and aromatic molecules, such as benzene. A very large variety of acceptor compounds have also been prepared, and are often based on Lewis acid intercalants such as the halogen Br_2 or halogen mixtures, metal chlorides, bromides, fluorides and oxyhalides, acidic oxides such as N_2O_5 and SO_3 and strong bronsted acids such as H_2SO_4 and HNO_3. In the intercalation process, the molecular intercalants generally remain molecular in form. From Figures 7(a) and 7(b) it can be seen that intercalation causes crystal dilatation along the c-axis: the larger the molecular intercalants, the larger the dilatation for compounds of comparable stage. In general, both chemical affinities and geometric constraints associated with intercalant size and intercalant bonding distances determine whether or not a given chemical species will intercalate. Many of these compounds are unstable in air, with donor compounds being easily oxidized and acceptors being easily desorbed. For this reason, most intercalation compounds require encapsulation to ensure chemical stability, though some compounds, such as graphite-$FeCl_3$ and graphite-$SbCl_5$, are relatively stable in air. In addition to the large number of chemical species that can be intercalated, a number of different types of graphite host materials are used for each of the various applications. From a structural point of view, the simplest host material is a single crystal graphite flake, such as those separated from the limestone rocks found in the Ticonderoga mines of New York State. Because flake dimensions are ~1 mm in diameter and only several hundredths of a millimeter in thickness, these materials often cannot be conveniently used for carrying out physical properties measurements. In such cases, samples of large physical dimensions based on highly oriented pyrolytic graphite (HOPG) are used (Moore 1973). HOPG is synthetic graphite formed by cracking a hydrocarbon at high temperature and subsequent heat treatment, often combined with the application of pressure. The resulting material is highly oriented along the c-axis (orientational deviations less than 18) but in the layer planes consists of a randomly ordered collection of crystallites of ~1 mm average diameter. For many physical measurements the greater flexibility in sample size provided by the HOPG host material is of greater importance than the more perfect ordering of the single crystal flakes. In fact,

HOPG has been the most common host material for graphite intercalation compounds during the recent period of active research. Another type of graphite host material is Kish graphite, obtained by the crystallization of carbon from molten steel during the steel manufacturing process. Kish graphite samples typically contain several large single crystallites, exhibiting much higher structural ordering than HOPG, but not quite as ordered or as chemically pure as natural single crystal flakes. On the other hand, Kish graphite samples are normally an order of magnitude greater in area and in thickness when compared with single crystal flakes. Though little use has so far been made of this host material, intercalation compounds based on Kish graphite can also be prepared.

1.5.2. Intercalation of graphite oxide

Graphite oxide is a typical two dimensional solid in bulk form, with strong covalent bonding within the layers. Weaker interlayer contact is made by hydrogen bonds between intercalated water molecules.[58-60] So far, many intercalated graphite oxide materials have been synthesized and their physicochemical properties investigated.[61-69] The interlayer space can be controlled by various size molecule intercalation processes. Matsuo et al. have used various kinds of surfactants with different chain lengths to synthesize surfactant-intercalated graphite oxide materials. These materials can be used as hosts for molecular recognition.[61] The exfoliation of graphite oxide particles occurs easily in dilute (alkaline) aqueous solution; polyaniline-intercalated graphite oxide material and nanometer compounds with particle properties have been synthesized by an exfoliation/adsorption process.[62-64] Using the hydrophilicity of graphite oxide, some polar organic molecules and polymers, such as alcohol,[65] poly(ethylene oxide) (PEO),[66, 67] poly(vinyl alcohol) (PVA),[67] poly(diallyldimethylammonium chloride) (PDDA),[68] poly(furfuryl alcohol) (PFA),[69] and even others, [58] can be easily inserted into its lamellae to form intercalated graphite oxide nanocomposites by different methods with different c-axis repeat distances. The existence of these polymers enables the physicochemical properties of graphite oxide to be greatly changed. Liu et al.[70] has synthesized a poly(vinyl acetate) intercalated graphite oxide nanocomposite using poly(vinyl acetate) (PVAc), with an oilsoluble polymer as guest molecules. The compound has a high stability against extraction by organic solvent due to a strong interaction between the graphite oxide layers and PVAc chains.[53, 70] Tetraalkylammonium cation have been use extensively to modify or delaminate layered hosts, [71-73] including expanded graphite sulfate.[74] The intercalation reaction of large organic ions into layered graphite oxide were conducted using tetraalkylammonium ions with different methylene chain lengths though ion-exchanging.[73]

In this report, we discuss about TBA cation intercalation into graphite oxide, mosaic monolayer fabrication with graphene from TBA intercalated graphite oxide and mechanism of mosaic monolayer.

2. Experimental section

2.1. Materials

Natural graphite having an average particle size of 74 μm was purchased from Bay Carbon (Michigan, USA). Chemical reagents used for the synthesis of graphite oxide, including phosphorus pentoxide (P_2O_5) and potassium permanganate ($KMnO_4$), were purchased from Sigma-Aldrich. Sulfuric acid (H_2SO_4) was obtained from Merck Chemicals (Darmstadt, Germany). Tetrabutylammonium hydroxide (TBAOH) was purchased from Sigma-Aldrich. The molecular weight cut (MWCO) of the dialysis tubing (Spectra/Por dialysis membrane) was 12–14 kD.

2.2. Preparation of graphite oxide

Graphite oxide was prepared from purified natural graphite (SP-1, Bay Carbon) by the modified Hummers' method.[75] The graphite powder (20 g) was put into an 80 °C solution of concentrated H_2SO_4 (30 mL), $K_2S_2O_8$ (10 g), and P_2O_5 (10 g). The resultant dark blue mixture was thermally isolated and allowed to cool to room temperature over a period of 6 h. The mixture was then carefully diluted with distilled water, filtered, and washed on the filter until the rinse water pH became neutral. The product was air dried at ambient temperature overnight. This pre-oxidized graphite was then subjected to oxidation by the Hummers' method. The pre-oxidized graphite powder (20 g) was put into cold concentrated H_2SO_4 (460 mL). $KMnO_4$ (60 g) was added gradually under stirring and cooling, and the temperature of the mixture was not allowed to reach 20 ^oC. The mixture was then stirred at 35 ^oC for 2 h, and distilled water (920 mL) was added. The oxidation temperature was changed to 20 ^oC and 27 ^oC respectively for the other samples. After 15 min, the reaction was terminated by the addition of a large amount of distilled water (2.8 L) and a 30 % H_2O_2 solution (50 mL), after which the colour of the mixture changes to bright yellow. The mixture was filtered and washed with a 1:10 HCl solution (5 L) in order to remove metal ions. The graphite oxide product was suspended in distilled water to give a viscous, brown dispersion, which was subjected to dialysis to completely remove metal ions and acids. After dialysis, it was centrifuged to make gel state graphite oxide. The final product was kept in dark place.

2.3. Intercalation reaction and exfoliation

Wet state of Graphite oxide (20 mg) was soaked in 1:3 TBAOH and water (20 mL) for 3 days. After soaking, the solution was dialyzed for 2 days. The solution was separated by centrifugation. The supernatant was graphene oxide (TGO) which was exfoliated from TBA intercalated graphite oxide (TIG). Intercalation and exfoliation of graphite oxide with detail is presented in scheme 1.

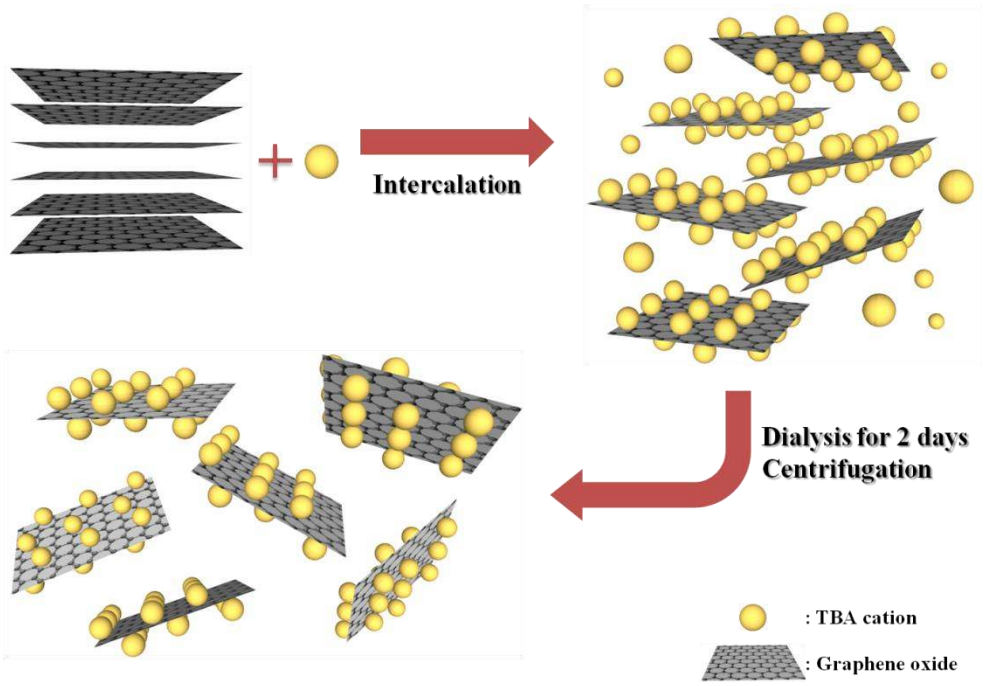

Scheme 1. Schematic flow diagram of intercalation of graphite oxide with TBA cation

2.4. Film fabrications

2.4.1. Spin coating

Silicon dioxide substrate was cleaned by piranha solution to remove any organic contamination and treated with oxygen plasma to introduce hydrophilic surface. TGO solution or graphene oxide (GO) solution was dropped on the silicon dioxide substrate which was loaded in a spin coater (ACE-200, Dong Ah Tech), maintained for 2 min as a waiting period, and spun at 3000 rpm for 30 sec.

2.4.2. Langmuir-Blodgett (LB)

Deionized water was used as the supporting subphase. When GO and TGO solution was directly applied onto a water surface, most of sheet sinks into water because TGO and GO sheets are well dispersed in water. Commonly used hydrophobic spreading solvent, such as chloroform or toluene, were not suitable since they do not disperse GO well. Methanol can yield a stable solution.[76] After addition of methanol in each solution, it disperses well and spreads on water rapidly. Methanol added in each solution with an optimal ratio of 1:5. The mixture solution was centrifuged at 3500 rpm for 10 min to remove aggregates. The LB trough (KN 2002, Nima Tech) was carefully cleaned and then filled with deionized water. The mixture solution was slowly dropped with speed of 100 μL/min to a total of 1.5 mL. Surface pressure was monitored using a tensiometer attached to a Wilhelmy plate. The film was compressed by barriers at a speed of 20 cm^2/min. Initial isotherms were taken after the film was allowed to equilibrate for at least 20 min after spreading. Isotherms in Figure have a zeroed baseline. The film was transferred to substrates at various points during the compression by vertically dipping the monolayer Oxygen plasma treated silicon dioxide substrate into the trough and slowly pulling in up (2 mm/min).

`

2.4.3. Measurements and characterization

For measuring interspace of graphite oxide and TBA-intercalated graphite oxide, X-ray diffraction (Normal X-ray diffraction; Bruker, USA) was used. The morphology and sheet size of GO and TGO was measured by scanning electron microscopy (SEM; FEI, USA). The thickness of GO and TGO on silicon dioxide substrate was measured by atomic force microscopy (AFM; Veeco, USA) in tapping mode. The element contents of GO and TGO was calculated for carbon, oxygen, nitrogen and hydrogen by an element analyzer, a Flash 2000 (EA; Thermo Scientific, Netherlands). The functional groups on GO and TGO were characterized by X-ray photoelectron spectroscopy (XPS; Thermo Fisher, K-alpha). UV-vis absorbance spectra of GO solution and TGO solution and transmittance of TGO film on quartz substrate was measured by a UV-Vis-NIR, a Cary 5000(Varian, USA). The resistance of the TGO film on quartz with different number of coating was measured by using the four-point probe method (AIT, CMT-SR 1000N). An isotherms of GO and TGO is measured by KSV-

NIMA Langmuir and Langmuir-Blodgett troughs. Zeta-potential of GO solution and TGO solution was measured by a Nano ZS (Malvern, UK). The molecular orientation of functional groups was measured using a fourier transform infrared spectroscopy (FT-IR; Agilent, USA) with a variable-angle reflectance accessory (Seagull). It was obtained using p-polarized light at an angle of incidence of 82°.

3. Result and discussion

3.1. TBA cation intercalation of graphite oxide

The graphite oxide was used at gel state for the intercalation reaction which was carried out at 25℃ for 3 days. In the present case, intercalant is TBAOH, with molecular formula $C_{16}H_{37}NO$ and with the following chemical structure:

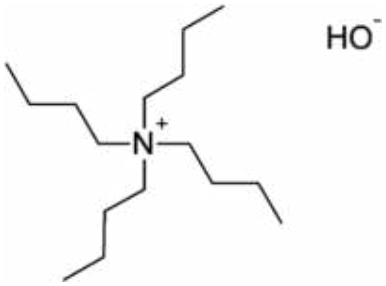

The XRD patterns of graphite oxide and TIG are shown in Figure 8. The XRD pattern of as prepared TIG (wet state) is presented in Figure 8(a). The pattern gives no clear peaks but only a broad diffraction halo. The broad halo is probably related to scattering from dispersed single sheets of graphene oxide (GO) and water.[73, 77, 78] It indicates that graphite oxide is exfoliated by TBA intercalation without any external power. The XRD patterns of the samples after drying 25℃ at for 2 days are shown in Figure 8(b). The XRD of dry state of sample was measured to know intercalation process was succeeded. The 2θ of graphite oxide and TIG are 10.67° and 6.34°. The corresponding interspacing for graphite oxide and TIG are found 8.3 Å and 13.9 Å respectively. The interspacing of graphite oxide is increased by 5.6 Å after the TBA intercalation. This is in accordance with the size of water and the TBA molecule (4.7 Å in flattened confirmation [79]). The single graphene sheet yields of samples from graphite oxide at both dry state and wet state are displayed in table 1. After dialysis, centrifugation was used to separate single graphene sheet from TBA intercalated graphite oxide. The yield of single graphene sheet (TGO) from TBA intercalated graphite oxide was calculated on difference between the concentration of solution before centrifugation and supernatant. And the yield of single graphene sheet (GO) from graphite oxide was calculated on the same method. The yield is given by the equation below.

$$\text{Yield}(\%) = \left(\frac{\text{concentration of supernatant}}{\text{concetration of the solution before centrifugation}}\right) \times 100$$

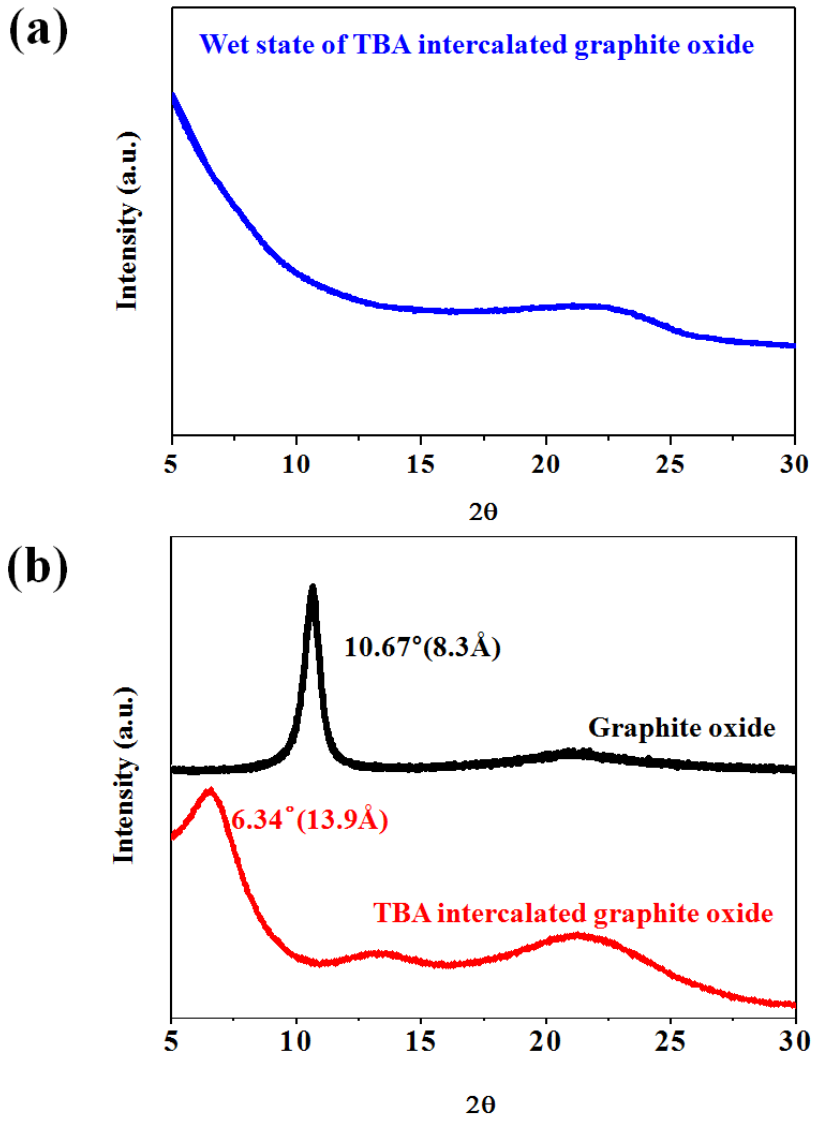

Figure 8. XRD patterns of graphite oxide. (a) Wet state of TBA intercalated graphite oxide; (b) Graphite oxide and TBA intercalated graphite a dried at 25℃ for 2day

The yield of samples starting with wet state of graphite oxide is ~8% higher than those starting with dry state of graphite oxide. Therefore wet state of graphite oxide was used in this experiment. The yield of graphene of graphite oxide and TIG both starting with wet state of graphene oxide is shown in table 2. The yield of single graphene sheet from graphite oxide and TIG is 18% and 46%. The yield of single graphene sheet from TIG is about 3 times higher than those from graphite oxide. This indicates that graphene from TBA intercalated graphite oxide is easier to exfoliate with bigger interspace.

3.2. The comparison of GO and TGO

Figure 9 shows the size and morphology of TGO sheet and graphene oxide sheet. Figure 9a and 9b is the sheet size histogram of GO and TGO. The sheet size of samples was counted with 500 SEM images. The average graphene sheet size of GO and those of TGO was 17.42 ± 10.33 and 19.87 ± 10.65 μm. The average graphene sheet size of TGO was 2.45 μm larger than those of GO. The largest sheet size of GO and TGO was 41.1 and 47.9 μm. The biggest sheet size of TGO is 6.8 μm larger than those of GO. AFM image of GO and TGO are shown in Figure 9c-f. The thickness of GO is 0.990 nm, which is general thickness of single sheet graphene oxide.[80-82] The thickness of TGO is 1.291 nm which is 0.301 nm thicker then GO single sheets due to residual TBA on graphene sheet. The increased thickness is similar to increased interspacing of dry state TIG. The element analyzer data (EA) of GO and TGO are shown in table 3. The content of nitrogen atom of GO and TGO is 0 w% and 2.131 w% respectively. It indicate that TBA cation was not removed completely due to interaction between GO and TBA cation. XPS was used to characterize the existence of TBA and the formation chemical bonds on the surface of GO and TGO (Figure 10). In contrast to XPS spectra of GO, XPS spectra of TGO has N1s peak in survey. The peak of GO in XPS spectra can be fit into four peaks centered at 284.18, 286.28, 287.68, and 290.18 eV, indicating that they are C-C, C-O, C=O and COOH group respectively. The XRD spectra of TGO can be deconvoluted into four peaks centered at 284.38, 285.56, 286.18 and 286.95 eV, indicating that they are C-C, C-O, C-N and C=O group respectively. The percentage of C-C peak in XPS spectra of GO is 49.24%. Whereas, the percentage of C-C peak in XPS spectra of TGO is increasing to 69.31%. In contrast, the percentage of functional group containing oxygen is decreasing. It indicated that TBA was not removed completely and TGO was reduced by intercalation. Figure 11 shows the photograph of TGO solution and GO solution and its UV-vis absorption spectrum. The color of GO is changed pale-yellow to dark-brown after TBA intercalation, suggesting the restoration of electronic conjugation. Although chemical reduction agent was not used, TBA intercalation caused the color change of GO solution. The color of TGO solution is consistent with an overall increase in absorption in the vicinity 238 nm absorption region, due to the presence of extended π-conjugation structure. The GO solution displayed an adsorption maximum at 231 nm which is due to $\pi \rightarrow \pi^*$ transition of aromatic C=C bonds and a shoulder around 300 nm which

	Single sheet yield (%)	
	Graphite oxide	TBA-graphite oxide
Starting from wet graphite oxide	9	33
Starting from dry graphite oxide	18	46

Table 1. Yield of single graphene sheet from graphite oxide and TIG started with wet and dry graphite oxide

Sample from wet graphite oxide	Single sheet yield (%)		
	first	second	third
Exfoliation from graphite oxide	13	13	18
Exfoliation from TBA-graphite oxide	33	31	46

Table 2. Yield of single graphene sheet from graphite oxide and TIG

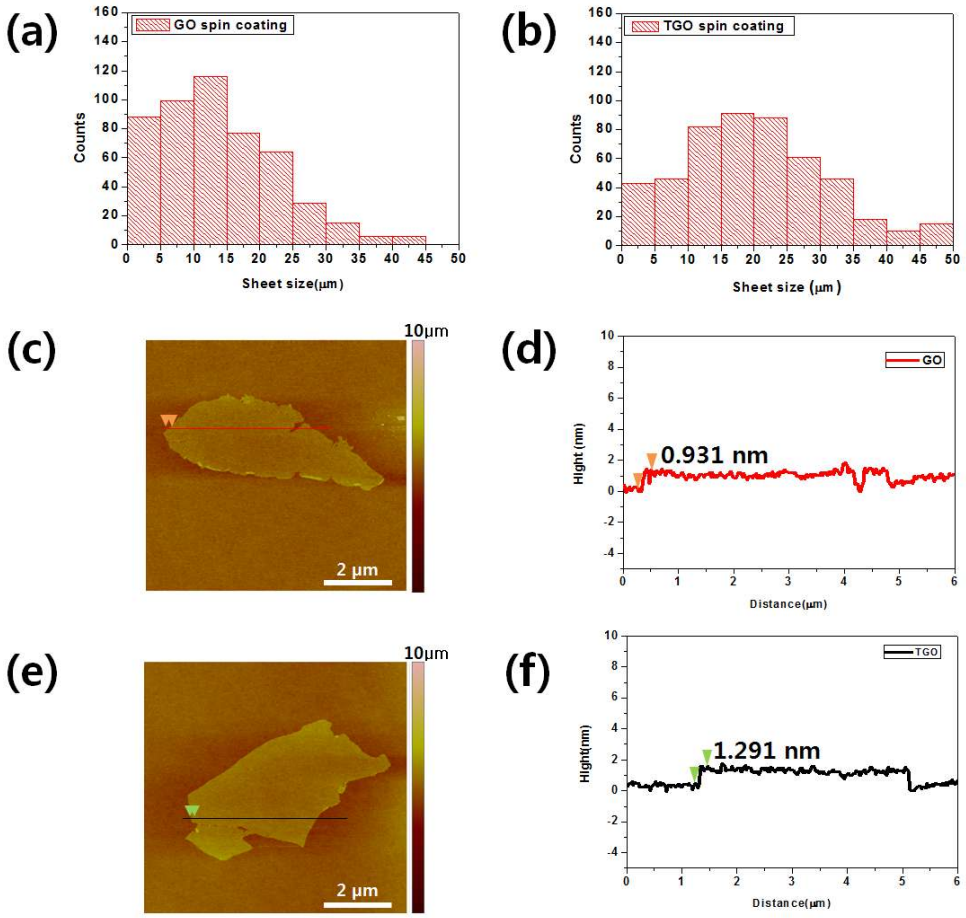

Figure 9. Characterization of graphene from TBA intercalated graphite oxide (TGO) and graphite oxide (GO). (a) Histogram of TGO sheet size. (Average size is 21.24± 9.11 μm.), (b) Histogram of TGO sheet size. (Average size is 18.4 ± 8.35 μm.), (c, e) Tapping mode atomic force microscopy images of GO and TGO, (d, f) The height profiles of GO and TGO. The corresponding thickness of GO and TGO sheets are 0.990 nm and 1.291 nm

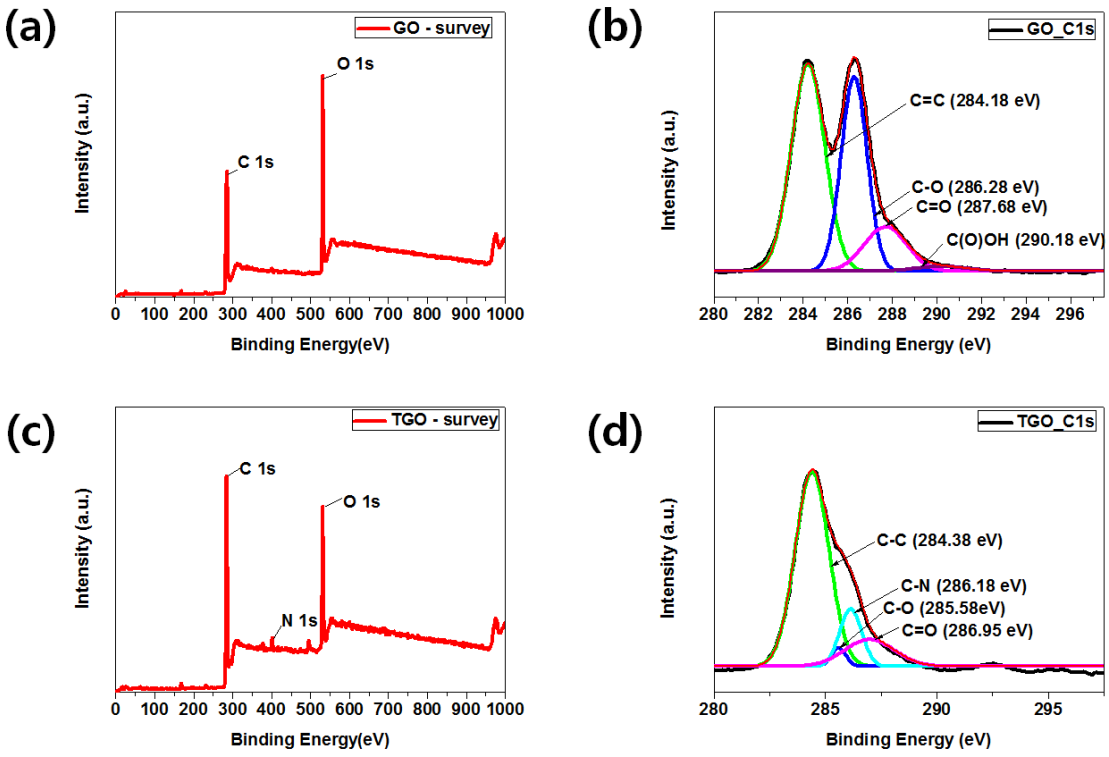

Figure 10. XPS of GO (a, b) and TGO (c, d), photograph of GO and TGO solution

corresponds to the π→n transition of the C=O bond. In case of TGO, the π→π* transition redshift from 231 nm to 235 nm and intensity of shoulder which corresponds to the π→n transition around 300 nm is decreasing.[83] It has been noted that, the absorption peak of a reduced graphene oxide by hydrazine shows a gradual redshift of 231 nm absorption peak to 235 nm with the increasing absorption in the whole spectral region in 2 mins. The absorption maximum finally shift to 270 nm and the intensity of shoulder around 300 nm disappear after 1 h.38 TGO has π→π* transition peak at 235 nm and less intensity of π→n transition, it rather indicates mild-reduction of GO.

3.3. Characterization of TGO film

The mosaic–like TGO monolayer was rinsed with water by spin coating at 3000 rpm. After spin coating and rinsing with water, it was observed that from the mosaic–like monolayer some sheets disappeared, indicating that the mosaic monolayers are not formed due to the interaction between TGO sheet and substrate rather interaction among TGO sheets. Also the density of the sheets was controlled by solution concentrations. The SEM image of TGO film with different concentration, 0.4, 0.85 and 1.0 mg/mL, is shown in Figure 12d-f. The SEM image of TGO mosaic-like monolayer on various substrates is shown in Figure 13. TGO mosaic-like monolayer was able to fabricate on hydrophobic Si wafer (Figure 13a) and CVD-grown graphene (Figure 13b). Also, the mosaic–like TGO monolayer was appeared on rough substrate such as Cu foil (Figure 13c) and Au/Si wafer (Figure 13d). Figure 14 exhibit the sheet resistance and transmittance of resulting TGO monolayers with number of coatings after annealing at 1050℃. The sheet resistance decreases with increasing number of TGO coating. The transmittance measured at 550 nm decreases gradually with increasing number of TGO coating. The resistance of TGO film was found to be 32.2 kΩ/□ at 96.09 % transmittance for 2 times coating. Although this result is better than the results of recent studies.[42, 46, 74, 84, 85] The high transmittance and low resistance with small number of coating with the edge of TGO sheets connect to each other can be useful for various applications like other transparent conducting oxides. The surface pressure-area isotherm was measure to know interaction among sheet. Figure 15 display surface pressure-area isotherms of GO and TGO. The GO films and TGO films were collected at different phase of compression by vertical dip-coating and imaged with SEM (insert). The surface pressure-area isotherm was measured with dropping sample in air-water interface in same volume (1.5 mL) and same concentration (0.4 mg/mL) of solution. As the area was decreased, the surface pressure started to rise and the sheets were pushed closer to each other. This can be attributed to the strong edge-to-edge electrostatic repulsion between neighboring sheets originating from the ionized carboxylic groups decorating their edges.[86] The isotherm of GO can be split into three region. Beyond ~180 cm^2 it shows the coexistence of a liquid-like (liquid-expanded, Le) and gaseous-analogue (G) phase. In this region, the GO sheet does not affect each other. Between 180 and 97.2 cm^2 it is a homogeneous Le phase and the surface pressure start increasing due to repulsion among sheets. After

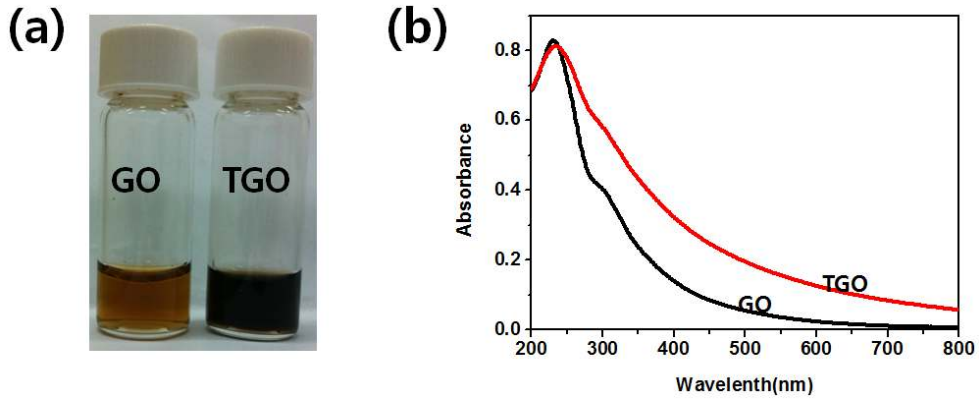

Figure 11. UV-vis of GO and TGO solution

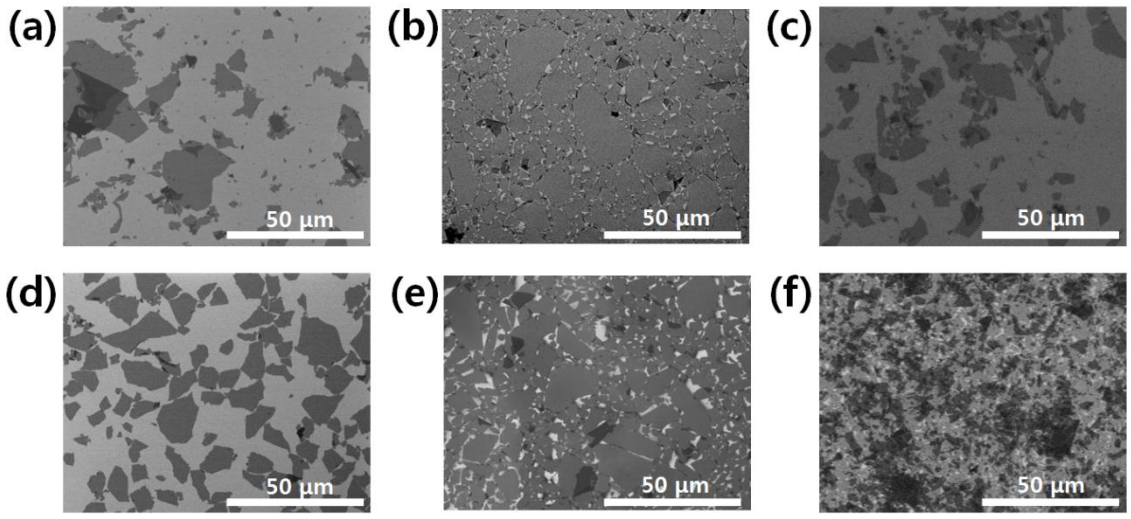

Figure 12. SEM of GO spin-coated film (a), TGO spin-coated film (b), TGO spin-coated film after water rinsing (e) and TGO spin-coated film with different concentration (d-f)

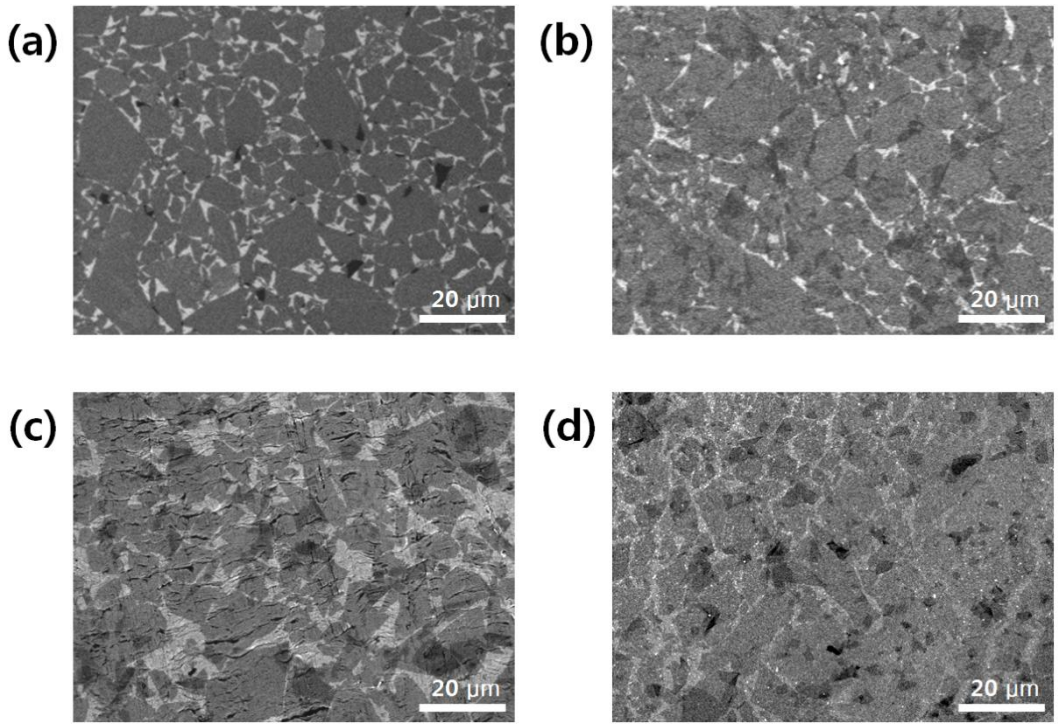

Figure 13. SEM of mosaic-like TGO film on Si wafer (a), CVD-grown graphene (b), Cu foil (c) and Au/Si wafer (d)

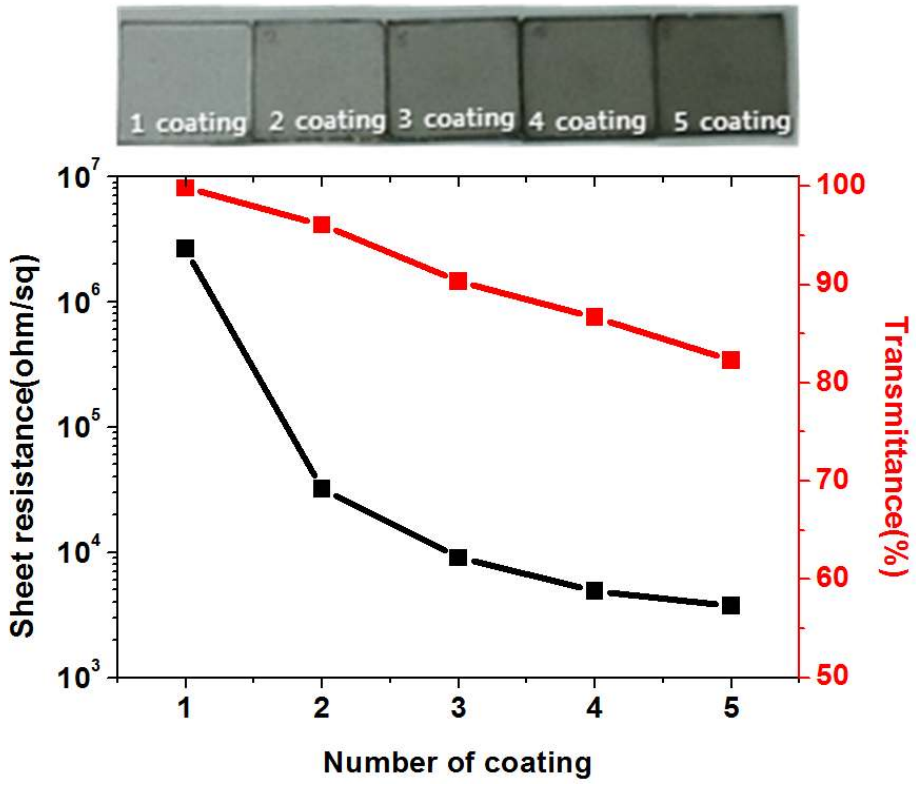

Figure 14. Sheet resistance and transmittance of TGO film after annealing in H_2 and Ar atmosphere at 1050 ℃. The top image shows a photograph for 1-5 coating of TGO deposited on a quartz substrate after annealing

97.2 cm^2 it has phase transition into the coexistence of the Le and a condensed Lc phase (liquid-condensed, Lc) and shows monolayer. In case of TGO, it has three parts. Beyond ~156.2 cm^2 it shows the coexistence of a Le and G phase. Between 156.2 and 52.98 cm^2 it shows the coexistence of the Le and a condensed Lc phase and shows monolayer. After 52.98 cm^2 phase transition into a condensed Lc phase is observed and there is overlapping of sheets. The isotherm of TGO does not show only Le phase unlike those of GO. It indicates that TGO sheets do not push each other as much as GO sheets while sheets are getting closer. The surface pressure of absorbing monolayer TGO and GO is in 0.1~ 33.2 and over 3.34 mN/m. The area of absorbing monolayer of GO and TGO is in less than 97.2 cm^2 and 52.98~156.2 cm^2. Although same volume and same concentration of GO and TGO solution was used, TBA monolayer has less surface pressure as compared to GO monolayer. Hence, the TGO monolayer was formed at less surface pressure then GO monolayer. The absence of Le phase in the isotherm of TGO is suggested that electrostatic repulsion between TGO sheets is weaker than those between GO sheets. The zeta-potential was used to measure of surface charge of GO and TGO. As prepared GO has -66.28 mV at pH 3.41. And as prepared TGO has -49.85 mV at pH 6.36. Although, both TGO and GO have negative charge, the TGO sheet has higher zeta-potential than GO sheet due to adsorption of TBA cation which has hydrophobic group on the GO. It indicates TBA cations are surrounding graphene sheet and as a result the repulsion among sheets is less. The SEM images of TGO and GO sheets show noticeable morphological differences. The TGO monolayer was formed at larger area then GO monolayer due to the difference of total sheet area. SEM images of GO and TGO show big difference. The LB film of TGO has large and small sheet whereas LB film of GO has only large sheets. The total sheets area of TGO is larger than GO. The difference of sheet size distributions of GO film and TGO film fabricated by spin-coating and Langmuir-Blodgett is shown in Figure 16. Figure 16(a) and (b) is sheet size histogram of GO with SEM images (insert) fabricated by spin-coating and LB. While spin-coated GO film has all size sheet (0~45 μm) but sheet size below 2.5 μm disappeared in GO LB film. The small GO sheet (~ 2.5 μm) is too hydrophilic to float on water due to small hydrophobic basal compared to hydrophilic edge. However, the TGO Langmuir-Blodgett film shows small TGO sheets. The small TGO sheets do not sink into water due to alkyl chain in TBA molecule surrounding TGO sheet. FT-IR reflection spectrum was studied to know the molecular orientation of functional groups on TGO film and GO film fabricated by spin-coating and LB in Figure 17. The samples were prepared on Au substrate for selectively detecting functional group oriented perpendicular to the substrate. The FTIR reflection spectra of GO fabricated by spin coating and LB is shown in Figure 17 (a). For FTIR reflection spectra of spin-coated GO, the following features are observed: a band around 1722 cm^{-1} (C=O stretching vibration), 1620 cm^{-1} (C=C stretching vibration) and 1106 cm^{-1} (C-O stretching vibration). The intensity of C=O stretching vibration and that of C=C stretching vibration is similar due to existing both functional groups vertically indicating functional group of C=C is arranged randomly. However, FTIR reflection spectra

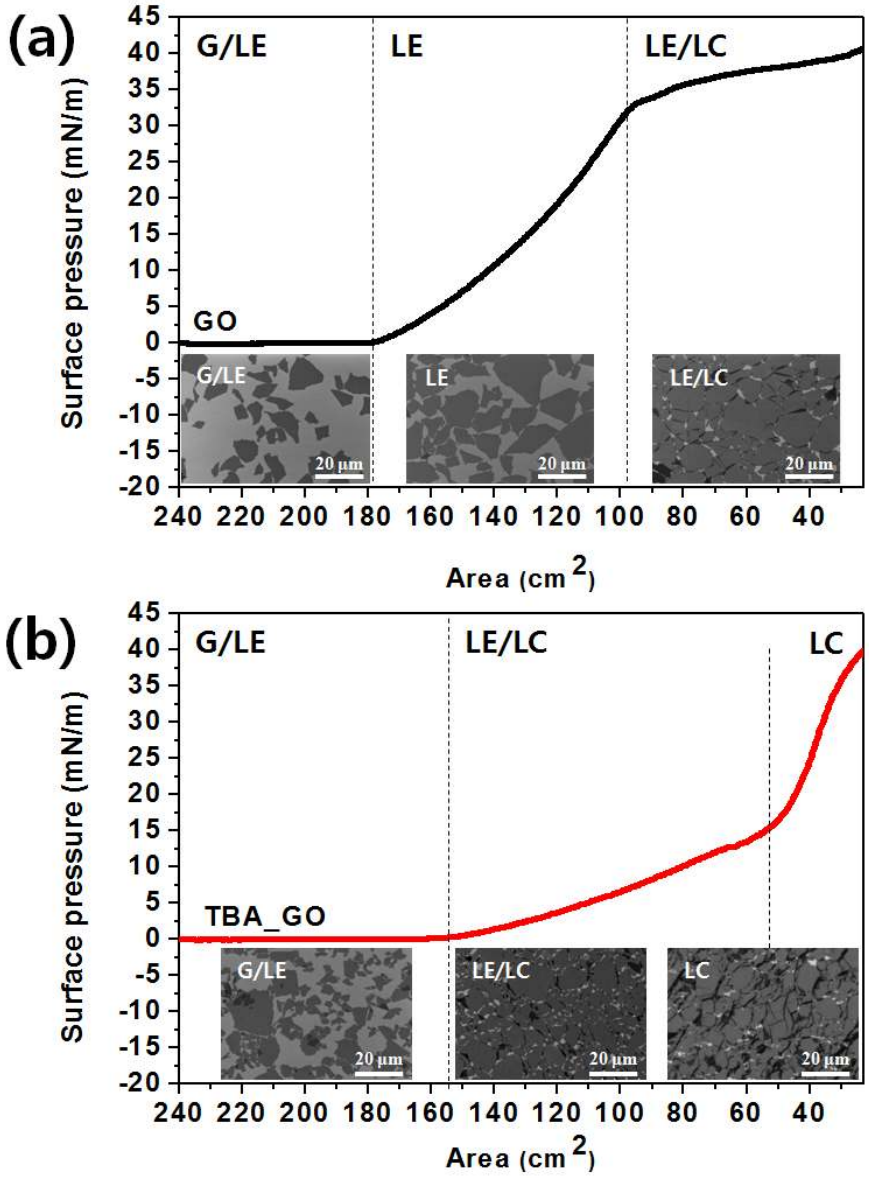

Figure 15. Surface pressure-Area isotherm of GO (a) and TGO (b), SEM image of GO layers and TGO layers collected on a silicon dioxide substrate at different stage of isothermal compression. (insert)

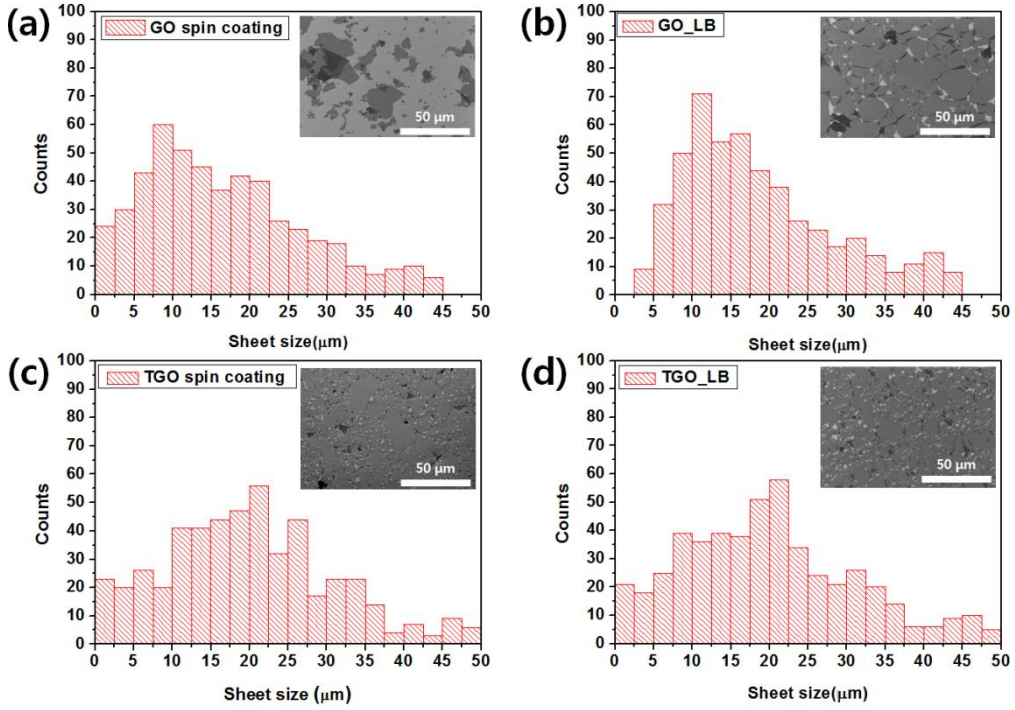

Figure 16. Histogram for sheet size distributions of GO film and TGO film fabricated by spin-coating and Langmuir-Blodgett

of LB monolayer of GO show relative higher intensity of C=O stretching vibration than that of C=C stretching vibration. It is indicated that GO LB monolayer has parallel basal plane (C=C bond) and vertical oxygen-contained functional group (C=O, C-O bond) to Au substrate and. It is well matched theory of LB that hydrophilic functional groups have perpendicular orientation at the air-water interface. The FTIR reflection spectra of TGO fabricated by both spin coating and LB show that higher intensity of than that C=O stretching vibration than that of C=C stretching vibration in Figure 17 (b). It is signified that TGO can be fabricated well orientated film with a simple spin coating.

4. Conclusion

In conclusion, we have shown high efficient method of synthesizing large size graphene oxide using TBAOH. Also, the mosaic thin film graphene oxide was fabricated due to low electrostatic repulsion among sheets by TBA cation adsorbed on GO sheet. Therefore, the successful mosaic monolayer fabrication in this study would enable various research and developments for real application since it has active functional group on very uniform monolayer and show low resistance in high transmittance after reduction process.

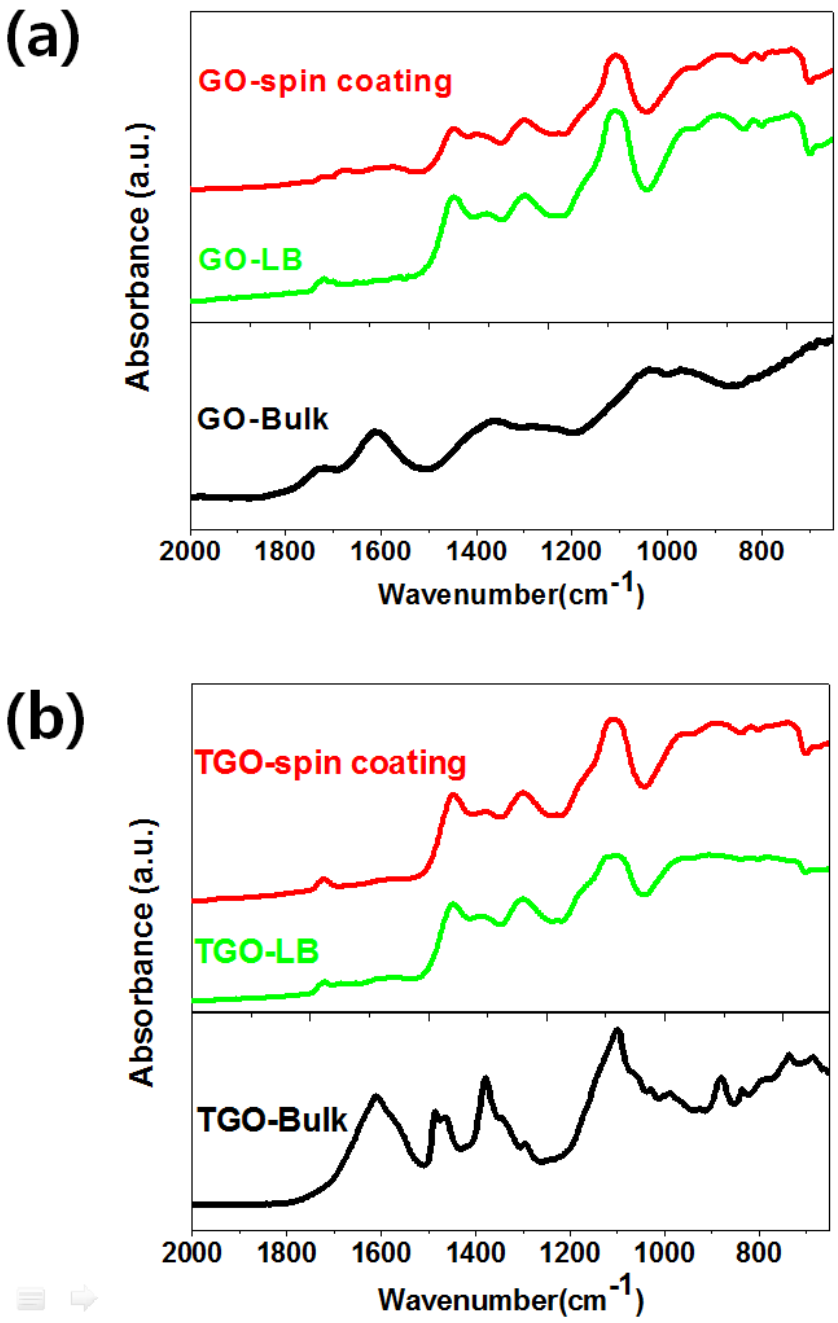

Figure 17. FT-IR reflection spectra of GO film (a) and TGO film (b)

References

1 Kroto, H. W., Heath, J. R., O'Brien, S. C., Curl, R. F. & Smalley, R. E. 1985. C 60: buckminsterfullerene. *Nature,* 318**,** 162-163.

2 Iijima, S. 1991. Helical microtubules of graphitic carbon. *Nature,* 354**,** 56-58.

3 Novoselov, K., Geim, A., Morozov, S., Jiang, D., Zhang, Y., Dubonos, S., Grigorieva, I. & Firsov, A. 2004. Electric field effect in atomically thin carbon films. *science,* 306**,** 666-669.

4 Mouras, S., Hamm, A., Djurado, D. & Cousseins, J. C. 1987. Synthesis of first stage graphite intercalation compounds with fluorides. *Revue de chimie minérale,* 24**,** 572-582.

5 Forbeaux, I., Themlin, J. M. & Debever, J. M. 1998. Heteroepitaxial graphite on 6H-SiC (0001): Interface formation through conduction-band electronic structure. *Physical Review B,* 58**,** 16396.

6 Novoselov, K., Geim, A. K., Morozov, S., Jiang, D., Grigorieva, M. I. K. I. V., Dubonos, S. & Firsov, A. 2005. Two-dimensional gas of massless Dirac fermions in graphene. *Nature,* 438**,** 197-200.

7 Zhang, Y., Tan, Y. W., Stormer, H. L. & Kim, P. 2005. Experimental observation of the quantum Hall effect and Berry's phase in graphene. *Nature,* 438**,** 201-204.

8 Wallace, P. 1947. The band theory of graphite. *Physical Review,* 71**,** 622.

9 Avouris, P., Chen, Z. & Perebeinos, V. 2007. Carbon-based electronics. *Nature Nanotechnology,* 2**,** 605-615.

10 Semenoff, G. W. 1984. Condensed-matter simulation of a three-dimensional anomaly. *Physical Review Letters,* 53**,** 2449-2452.

11 Novoselov, K., Geim, A., Morozov, S., Jiang, D., Grigorieva, M. I. K. I. V., Dubonos, S. & Firsov, A. 2005. Two-dimensional gas of massless Dirac fermions in graphene. *Nature,* 438**,** 197-200.

12 Novoselov, K. S., Jiang, Z., Zhang, Y., Morozov, S., Stormer, H., Zeitler, U., Maan, J., Boebinger, G., Kim, P. & Geim, A. 2007. Room-temperature quantum Hall effect in graphene. *science,* 315**,** 1379-1379.

13 Klitzing, K., Dorda, G. & Pepper, M. 1980. New method for high-accuracy determination of the fine-structure constant based on quantized Hall resistance. *Physical Review Letters,* 45**,** 494-497.

14 Geim, A. K. & Novoselov, K. S. 2007. The rise of graphene. *Nature materials,* 6**,** 183-191.

15 Lee, C., Wei, X., Kysar, J. W. & Hone, J. 2008. Measurement of the elastic properties and intrinsic strength of monolayer graphene. *science,* 321**,** 385-388.

16 Frank, I., Tanenbaum, D., Van Der Zande, A. & McEuen, P. 2007. Mechanical properties of suspended graphene sheets. *Journal of Vacuum Science & Technology B: Microelectronics and Nanometer Structures,* 25**,** 2558.

17 Kuzmenko, A., Van Heumen, E., Carbone, F. & Van der Marel, D. 2008. Universal optical conductance of graphite. *Physical Review Letters,* 100**,** 117401.

18 Nair, R. R., Blake, P., Grigorenko, A. N., Novoselov, K. S., Booth, T. J., Stauber, T., Peres, N. M. R. & Geim, A. K. 2008. Fine Structure Constant Defines Visual Transparency of Graphene. *Science,* 320**,** 1308.

19 Zhang, Y., Tang, T. T., Girit, C., Hao, Z., Martin, M. C., Zettl, A., Crommie, M. F., Shen, Y. R. & Wang, F. 2009. Direct observation of a widely tunable bandgap in bilayer graphene. *Nature,* 459**,** 820-823.

20 Liu, J., Wright, A., Zhang, C. & Ma, Z. 2008. Strong terahertz conductance of graphene nanoribbons under a magnetic field. *Applied Physics Letters,* 93**,** 041106.

21 Balandin, A. A., Ghosh, S., Bao, W., Calizo, I., Teweldebrhan, D., Miao, F. & Lau, C. N. 2008. Superior thermal conductivity of single-layer graphene. *Nano letters,* 8**,** 902-907.

22 Saito, K., Nakamura, J. & Natori, A. 2007. Ballistic thermal conductance of a graphene sheet. *Physical Review B,* 76**,** 115409.

23 Novoselov, K., Jiang, D., Schedin, F., Booth, T., Khotkevich, V., Morozov, S. & Geim, A.

2005. Two-dimensional atomic crystals. *Proceedings of the National Academy of Sciences of the United States of America,* 102**,** 10451.
24 Park, S. & Ruoff, R. S. 2009. Chemical methods for the production of graphenes. *Nature Nanotechnology,* 4**,** 217-224.
25 Li, D., Müller, M. B., Gilje, S., Kaner, R. B. & Wallace, G. G. 2008. Processable aqueous dispersions of graphene nanosheets. *Nature nanotechnology,* 3**,** 101-105.
26 Dikin, D. A., Stankovich, S., Zimney, E. J., Piner, R. D., Dommett, G. H. B., Evmenenko, G., Nguyen, S. B. T. & Ruoff, R. S. 2007. Preparation and characterization of graphene oxide paper. *Nature,* 448**,** 457-460.
27 Berger, C., Song, Z., Li, T., Li, X., Ogbazghi, A. Y., Feng, R., Dai, Z., Marchenkov, A. N., Conrad, E. H. & Phillip, N. 2004. Ultrathin epitaxial graphite: 2D electron gas properties and a route toward graphene-based nanoelectronics. *The Journal of Physical Chemistry B,* 108**,** 19912-19916.
28 Berger, C., Song, Z., Li, X., Wu, X., Brown, N., Naud, C., Mayou, D., Li, T., Hass, J. & Marchenkov, A. N. 2006. Electronic confinement and coherence in patterned epitaxial graphene. *Science,* 312**,** 1191.
29 Kedzierski, J., Hsu, P. L., Healey, P., Wyatt, P. W., Keast, C. L., Sprinkle, M., Berger, C. & de Heer, W. A. 2008. Epitaxial graphene transistors on SiC substrates. *Electron Devices, IEEE Transactions on,* 55**,** 2078-2085.
30 Moon, J., Curtis, D., Hu, M., Wong, D., McGuire, C., Campbell, P., Jernigan, G., Tedesco, J., VanMil, B. & Myers-Ward, R. 2009. Epitaxial-graphene RF field-effect transistors on Si-face 6H-SiC substrates. *Electron Device Letters, IEEE,* 30**,** 650-652.
31 Reina, A., Jia, X., Ho, J., Nezich, D., Son, H., Bulovic, V., Dresselhaus, M. S. & Kong, J. 2008. Large area, few-layer graphene films on arbitrary substrates by chemical vapor deposition. *Nano Letters,* 9**,** 30-35.
32 Kim, K. S., Zhao, Y., Jang, H., Lee, S. Y., Kim, J. M., Ahn, J. H., Kim, P., Choi, J. Y. & Hong, B. H. 2009. Large-scale pattern growth of graphene films for stretchable transparent electrodes. *Nature,* 457**,** 706-710.
33 Li, X., Cai, W., An, J., Kim, S., Nah, J., Yang, D., Piner, R., Velamakanni, A., Jung, I. & Tutuc, E. 2009. Large-area synthesis of high-quality and uniform graphene films on copper foils. *Science,* 324**,** 1312.
34 Bae, S., Kim, H., Lee, Y., Xu, X., Park, J. S., Zheng, Y., Balakrishnan, J., Lei, T., Kim, H. R. & Song, Y. I. 2010. Roll-to-roll production of 30-inch graphene films for transparent electrodes. *Nature nanotechnology,* 5**,** 574-578.
35 Hong, G., Wu, Q. H., Ren, J. & Lee, S. T. 2012. Mechanism of non-metal catalytic growth of graphene on silicon. *Applied Physics Letters,* 100**,** 231604-231604-5.
36 Dikin, D. A., Stankovich, S., Zimney, E. J., Piner, R. D., Dommett, G. H. B., Evmenenko, G., Nguyen, S. T. & Ruoff, R. S. 2007. Preparation and characterization of graphene oxide paper. *Nature,* 448**,** 457-460.
37 Xu, Y., Bai, H., Lu, G., Li, C. & Shi, G. 2008. Flexible Graphene Films via the Filtration of Water-Soluble Noncovalent Functionalized Graphene Sheets. *Journal of the American Chemical Society,* 130**,** 5856-5857.
38 Li, D., Muller, M. B., Gilje, S., Kaner, R. B. & Wallace, G. G. 2008. Processable aqueous dispersions of graphene nanosheets. *Nat Nano,* 3**,** 101-105.
39 Kong, B.-S., Yoo, H.-W. & Jung, H.-T. 2009. Electrical Conductivity of Graphene Films with a Poly(allylamine hydrochloride) Supporting Layer. *Langmuir,* 25**,** 11008-11013.
40 Park, S., An, J., Jung, I., Piner, R. D., An, S. J., Li, X., Velamakanni, A. & Ruoff, R. S. 2009. Colloidal Suspensions of Highly Reduced Graphene Oxide in a Wide Variety of Organic Solvents. *Nano Letters,* 9**,** 1593-1597.
41 Kong, B.-S., Geng, J. & Jung, H.-T. 2009. Layer-by-layer assembly of graphene and gold nanoparticles by vacuum filtration and spontaneous reduction of gold ions. *Chemical Communications***,** 2174-2176.
42 Wang, X., Zhi, L. & Mullen, K. 2007. Transparent, Conductive Graphene Electrodes for Dye-Sensitized Solar Cells. *Nano letters,* 8**,** 323-327.

43 Zhu, Y., Cai, W., Piner, R. D., Velamakanni, A. & Ruoff, R. S. 2009. Transparent self-assembled films of reduced graphene oxide platelets. *Applied Physics Letters,* 95**,** 103104.
44 Yamaguchi, H., Eda, G., Mattevi, C., Kim, H. & Chhowalla, M. 2010. Highly Uniform 300 mm Wafer-Scale Deposition of Single and Multilayered Chemically Derived Graphene Thin Films. *ACS Nano,* 4**,** 524-528.
45 Wang, X., Zhi, L., Tsao, N., Zcaron, Tomovi, e., cacute, Li, J. & Müllen, K. 2008. Transparent Carbon Films as Electrodes in Organic Solar Cells13. *Angewandte Chemie International Edition,* 47**,** 2990-2992.
46 Becerril, H. A., Mao, J., Liu, Z., Stoltenberg, R. M., Bao, Z. & Chen, Y. 2008. Evaluation of solution-processed reduced graphene oxide films as transparent conductors. *Acs Nano,* 2**,** 463-470.
47 Yanyu, L. & et al. 2009. Transparent, highly conductive graphene electrodes from acetylene-assisted thermolysis of graphite oxide sheets and nanographene molecules. *Nanotechnology,* 20**,** 434007.
48 Li, X., Zhang, G., Bai, X., Sun, X., Wang, X., Wang, E. & Dai, H. 2008. Highly conducting graphene sheets and Langmuir-Blodgett films. *Nat Nano,* 3**,** 538-542.
49 Cote, L. J., Kim, F. & Huang, J. 2008. Langmuir−Blodgett Assembly of Graphite Oxide Single Layers. *Journal of the American Chemical Society,* 131**,** 1043-1049.
50 Kim, K. S., Zhao, Y., Jang, H., Lee, S. Y., Kim, J. M., Kim, K. S., Ahn, J.-H., Kim, P., Choi, J.-Y. & Hong, B. H. 2009. Large-scale pattern growth of graphene films for stretchable transparent electrodes. *Nature,* 457**,** 706-710.
51 Gao, W., Alemany, L. B., Ci, L. & Ajayan, P. M. 2009. New insights into the structure and reduction of graphite oxide. *Nat Chem,* 1**,** 403-408.
52 Shen, J., Hu, Y., Li, C., Qin, C., Shi, M. & Ye, M. 2009. Layer-by-Layer Self-Assembly of Graphene Nanoplatelets. *Langmuir,* 25**,** 6122-6128.
53 Kovtyukhova, N. I., Ollivier, P. J., Martin, B. R., Mallouk, T. E., Chizhik, S. A., Buzaneva, E. V. & Gorchinskiy, A. D. 1999. Layer-by-Layer Assembly of Ultrathin Composite Films from Micron-Sized Graphite Oxide Sheets and Polycations. *Chemistry of Materials,* 11**,** 771-778.
54 Tredgold, R. 1999. The physics of Langmuir-Blodgett films. *Reports on Progress in Physics,* 50**,** 1609.
55 Holmberg, K., Shah, D. O. & Schwuger, M. J. 2002. *Handbook of applied surface and colloid chemistry,* Chichester, England ; New York, Wiley.
56 Barnes, G. & Gentle, I. 2011. *Interfacial science : an introduction,* Oxford, Oxford University Press.
57 Petty, M. C. 1996. *Langmuir-Blodgett films: an introduction*, Cambridge University Press.
58 Nakajima, T., Mabuchi, A. & Hagiwara, R. 1988. A new structure model of graphite oxide. *Carbon,* 26**,** 357-361.
59 Lerf, A., He, H., Forster, M. & Klinowski, J. 1998. Structure of Graphite Oxide Revisited. *The Journal of Physical Chemistry B,* 102**,** 4477-4482.
60 Mermoux, M., Chabre, Y. & Rousseau, A. 1991. FTIR and ^{13}C NMR study of graphite oxide. *Carbon,* 29**,** 469-474.
61 Matsuo, Y., Niwa, T. & Sugie, Y. 1999. Preparation and characterization of cationic surfactant-intercalated graphite oxide. *Carbon,* 37**,** 897-901.
62 Inagaki, M. & Suwa, T. 2001. Pore structure analysis of exfoliated graphite using image processing of scanning electron micrographs. *Carbon,* 39**,** 915-920.
63 Cassagneau, T. & Fendler, J. H. 1999. Preparation and layer-by-layer self-assembly of silver nanoparticles capped by graphite oxide nanosheets. *The Journal of Physical Chemistry B,* 103**,** 1789-1793.
64 Matsuo, Y., Tahara, K. & Sugie, Y. 1997. Structure and thermal properties of poly (ethylene oxide)-intercalated graphite oxide. *Carbon,* 35**,** 113-120.
65 Cassagneau, T., Guérin, F. & Fendler, J. H. 2000. Preparation and characterization of ultrathin films layer-by-layer self-assembled from graphite oxide nanoplatelets and polymers. *Langmuir,* 16**,** 7318-7324.
66 Matsuo, Y., Tahara, K. & Sugie, Y. 1996. Synthesis of poly(ethylene oxide)-intercalated

graphite oxide. *Carbon,* 34**,** 672-674.
67 Matsuo, Y., Hatase, K. & Sugie, Y. 1998. Preparation and characterization of poly (vinyl alcohol)-and Cu (OH) 2-poly (vinyl alcohol)-intercalated graphite oxides. *Chemistry of materials,* 10**,** 2266-2269.
68 Kotov, N. A., Dekany, I. & Fendler, J. H. 2004. Ultrathin graphite oxide–polyelectrolyte composites prepared by self-assembly: Transition between conductive and non-conductive states. *Advanced Materials,* 8**,** 637-641.
69 Kyotani, T., Moriyama, H. & Tomita, A. 1997. High temperature treatment of polyfurfuryl alcohol/graphite oxide intercalation compound. *Carbon,* 35**,** 1185-1187.
70 Liu, P., Gong, K., Xiao, P. & Xiao, M. 2000. Preparation and characterization of poly (vinyl acetate)-intercalated graphite oxide nanocomposite. *J. Mater. Chem.,* 10**,** 933-935.
71 Omomo, Y., Sasaki, T., Wang, L. & Watanabe, M. 2003. Redoxable nanosheet crystallites of MnO2 derived via delamination of a layered manganese oxide. *Journal of the American Chemical Society,* 125**,** 3568-3575.
72 Shiguihara, A. L., Bizeto, M. A. & Constantino, V. R. L. 2007. Exfoliation of layered hexaniobate in tetra (*n*-butyl) ammonium hydroxide aqueous solution. *Colloids and Surfaces A: Physicochemical and Engineering Aspects,* 295**,** 123-129.
73 Liu, Z., Wang, Z. M., Yang, X. & Ooi, K. 2002. Intercalation of organic ammonium ions into layered graphite oxide. *Langmuir,* 18**,** 4926-4932.
74 Li, X., Zhang, G., Bai, X., Sun, X., Wang, X., Wang, E. & Dai, H. 2008. Highly conducting graphene sheets and Langmuir–Blodgett films. *Nature Nanotechnology,* 3**,** 538-542.
75 Hummers, W. S. & Offeman, R. E. 1958. Preparation of Graphitic Oxide. *Journal of the American Chemical Society,* 80**,** 1339-1339.
76 Kim, F., Cote, L. J. & Huang, J. 2010. Graphene Oxide: Surface Activity and Two-Dimensional Assembly. *Advanced Materials,* 22**,** 1954-1958.
77 Srivastava, S., Jain, K., Singh, V., Singh, S., Vijayan, N., Dilawar, N., Gupta, G. & Senguttuvan, T. 2012. Faster response of NO2 sensing in graphene–WO3 nanocomposites. *Nanotechnology,* 23**,** 205501.
78 Zhou, Y., Xu, F., Jiang, G., Wang, X., Hu, R., Wang, R., Xi, X., Wang, S., Wang, T. & Chen, W. 2012. Superhydrophobic and high adhesive performance of functionalized graphene films. *Powder Technology*.
79 Sirisaksoontorn, W., Adenuga, A. A., Remcho, V. T. & Lerner, M. M. 2011. Preparation and Characterization of a Tetrabutylammonium Graphite Intercalation Compound. *Journal of the American Chemical Society,* 133**,** 12436-12438.
80 Eda, G., Fanchini, G. & Chhowalla, M. 2008. Large-area ultrathin films of reduced graphene oxide as a transparent and flexible electronic material. *Nature Nanotechnology,* 3**,** 270-274.
81 Dang, T. T., Pham, V. H., Hur, S. H., Kim, E. J., Kong, B. S. & Chung, J. S. 2012. Superior dispersion of highly reduced graphene oxide in N, N-dimethylformamide. *Journal of colloid and interface science*.
82 Gómez-Navarro, C., Weitz, R. T., Bittner, A. M., Scolari, M., Mews, A., Burghard, M. & Kern, K. 2007. Electronic transport properties of individual chemically reduced graphene oxide sheets. *Nano letters,* 7**,** 3499-3503.
83 Ang, P. K., Wang, S., Bao, Q., Thong, J. T. L. & Loh, K. P. 2009. High-Throughput Synthesis of Graphene by Intercalation−Exfoliation of Graphite Oxide and Study of Ionic Screening in Graphene Transistor. *Acs Nano,* 3**,** 3587-3594.
84 Park, K. H., Kim, B. H., Song, S. H., Kwon, J., Kong, B. S., Kang, K. & Jeon, S. 2012. Exfoliation of Non-Oxidized Graphene Flakes for Scalable Conductive Film. *Nano letters,* 12**,** 2871-2876.
85 Lee, D. W., Hong, T.-K., Kang, D., Lee, J., Heo, M., Kim, J. Y., Kim, B.-S. & Shin, H. S. 2011. Highly controllable transparent and conducting thin films using layer-by-layer assembly of oppositely charged reduced graphene oxides. *Journal of Materials Chemistry,* 21**,** 3438-3442.
86 Kim, F., Cote, L. J. & Huang, J. 2010. Graphene Oxide: Surface Activity and Two-Dimensional Assembly. *Advanced Materials,* 22**,** 1954-1958.

Acknowledgements

2년 가까이 공부한 석사생활이 끝나가면서, 후회되는 부분도 참 많고 감사한 것도 너무나 많다는 생각이 듭니다. 열정이 가득했던 처음 몇 달 동안은 마냥 즐거웠고, 생각보다 결과가 나오지 않아 우울했을 때도 있었고 실험을 하고 공부를 하는 것이 마냥 싫을 때도 있었습니다. 근거 없는 자신감에 가득 차있던 저를 스스로 되돌아보는 계기가 되고 제가 어떤 사람인지 어떤 것을 잘하고 어떤 것을 잘 못하는지에 대해 생각할 수 있는 시간이었습니다. 그리고 사람을 대하는 방법에 대해서도 배울 수 있었습니다. 살면서 지난 2년 동안 서울을 제일 많이 가보았던 것 같습니다. ^^

제가 교수님을 잘 따라갈 때나 뒤쳐질 때나 멈춰있을 때도 언제나 변치 않고 저를 이끌어주시던 교수님, 너무나 감사 드립니다. Shin's training에서 높은 grade를 받지는 못하고 졸업을 해서 후회가 되지만, 저는 많은 것을 배울 수 있는 시간이었습니다.

힘들 때마다 달래주고 하나밖에 없는 여자 후배라고 많이 챙겨주고 막 나가는 저를 잘 잡아주던 지은 언니, 제가 언니가 잘 해주는 만큼 잘 해드리지 못해서 죄송해요. 제 코가 석자여서 언니도 못 챙기는 동생 예쁘게 봐주셔서 너무 고마워요, 언니ㅋ. 옆에서 항상 챙겨주시고 잘 챙겨주고 많은 부분에서 멘토가 되어준 동우오빠 진짜 thank you! 나동일 때도 그의 팬인 동우 오빠일 때도 오빤 진짜 멋진 선배인 것 같아요 ㅋㅋ. 실험에 대한 팁을 많이 가르쳐 준 병환 오빠, flexible한 실험에 대해 많은 생각을 하게 해줘서 고마워요. 꼼꼼하고 차분한 아랑오빠, 오빠의 실험을 보면서 나도 차분해져야 하는데 라는 생각을 많이 했었어요. 가기 전에 오빠 곳간 채워드릴게요ㅎ. 누나를 잘 챙겨준 관우, 광우, 성인이, 성준아 고마워! 우리 오피스 오빠들 많은 도움 주셔서 고맙습니다. 그리고 정인 언니, 저 처음에 실험실에 와서 마음을 잡지 못하고 있을 때, 하나언니랑 저 위로도 해주시고 좋은 말씀 많이 해주셔서 진짜 고맙습니다.

그리고 공부하는 저의 기분을 맞춰주신다고 저보다 더 힘드셨을 부모님 항상 감사하고 사랑합니다.